9-2021

Catastrophic Beach Sand Losses Due to Erosion from Predicted Future Sea Level Rise (0.5–1.0 m), Based on Increasing Submarine Accommodation Spaces in the High-Wave-Energy Coast of the Pacific Northwest, Washington, Oregon, and Northern California, USA

Curt D. Peterson
Portland State University, curt.d.peterson@gmail.com

Don Joseph Pettit
Portland State University

Kara E. P. Kingen
Portland State University, kkingen@pdx.edu

Sandy Vanderburgh
Kwantlen Polytechnic University

Chuck Rosenfeld
Oregon State University

Citation Details

Peterson, C. D., Pettit, D. J., Kingen, K., Vanderburgh, S., & Rosenfeld, C. (2021). Catastrophic beach sand losses due to erosion from predicted future sea level rise (0.5–1.0 m), based on increasing submarine accommodation spaces in the high-wave-energy coast of the Pacific Northwest, Washington, Oregon, and Northern California, USA. Marine Geology, 439, 106555.

Marine Geology 439 (2021) 106555

Contents lists available at ScienceDirect

Marine Geology

journal homepage: www.elsevier.com/locate/margo

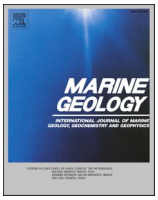

Catastrophic beach sand losses due to erosion from predicted future sea level rise (0.5–1.0 m), based on increasing submarine accommodation spaces in the high-wave-energy coast of the Pacific Northwest, Washington, Oregon, and Northern California, USA

Curt D. Peterson [a,*], Don J. Pettit [a], Kara Kingen [a], Sandy Vanderburgh [b], Chuck Rosenfeld [c]

[a] Geology Department, Portland State University, Portland 97207, USA
[b] Kwantlen Polytechnic University, Surrey V3W2M8, Canada
[c] Oregon State University, Corvallis 97331, USA

ARTICLE INFO

Editor: Edward Anthony
Potentile
Beach
Sand
Erosion
From
Predicted
Future
Sea
Level
Rise

ABSTRACT

The U.S. Pacific Northwest (PNW) coastline (1000 km) has been analyzed for conditions that could impact beach erosion from potential near-future (100 year) sea level rise (SLR). Heavy mineral analysis of river, beach, and shelf samples (n = 105) establish the sources of the beach deposits. River bedload discharge and intervening estuarine sinks for river sand supplies (n = 31) were normalized to the one century time interval. Twenty-six subcell beaches (657 km in combined length) were surveyed (153 profiles) for beach sand widths (20–412 m) and sand cross-sectional areas (20–1810 m^2) above wave-cut platforms and/or 0 m tidal datum. Cross-sectional areas were multiplied by beach segments to yield subcell beach sand volumes (0.4×10^6 m^3–35.8×10^6 m^3 ± 20% uncertainty). Innermost-shelf profiles were measured for distance to the 100-year depth of closure (30 m) to digitize the areas of inner-shelf accommodation space. Both innermost-shelf and estuarine accommodation space volumes for beach sand displacements were established for 0.5 and 1.0 m SLR. The existing subcell beach sand volumes and computed new beach sand supplies (rivers and longshore transport) were subtracted from the estimated sand volumes lost to submarine accommodation spaces to establish potential beach sand deficits from near-future SLR. Of the 26 surveyed active-beaches, some 60% and 80% (by length) are predicted to be lost, respectively, from the 0.5 m and 1.0 m SLR or equivalent littoral sand sedimentation in submarine accommodation spaces. Projected losses reach 90% for all PNW beaches (~900 km total length) from 1.0 m SLR. The computed beach sand deficits are used to estimate soft-sand retreat distances or erosional beach step backs (50–590 m ± 35% uncertainty) in unrevetted barrier spit and beach/dune deflation plains from 1.0 m SLR. Such empirical accommodation space analyses should have worldwide relevance to predicting beach erosion from near-future SLR.

1. Introduction

Sandy beaches in the high-wave-energy coastline of the U.S. Pacific Northwest (PNW) region of the northeast Pacific Ocean (Fig. 1) face potentially adverse conditions of widespread erosion from potential sea level rise (SLR). Predictions of near-future SLR rise currently range from 0.5 to 1.0 m within the next century (DeConto and Pollard, 2016; Mengel et al., 2016; Kopp et al., 2019; Bamber et al., 2019; Horton et al., 2020). Many approaches to estimating beach erosion from SLR have been proposed (Bruun, 1962; Bruun, 1988; Cooper and Pilkey, 2004; Walkden and Dickson, 2008; Masselink and Russell, 2013), but few of them address the complexities of beaches in the high-wave-energy active-margin setting of the U.S. PNW region. Beaches in the PNW region vary widely in active-beach widths, sea cliff or barrier/dunes in back-beach areas, river sand supply, estuary sand sinks, net longshore transport, bounding headlands, and inner-shelf gradients (Peterson et al., 1991; Peterson et al., 1994). Averaged beach widths within headland bounded subcells range from 60 to 100 m in some sea cliff-backed beaches to as much as 200–300 m in widely prograded barrier-spit and beach plain settings in the Columbia River Littoral Cell

* Corresponding author.
E-mail addresses: curt.d.peterson@gmail.com (C.D. Peterson), sandy.vanderburgh@kpu.ca (S. Vanderburgh).

https://doi.org/10.1016/j.margeo.2021.106555
Received 5 April 2021; Received in revised form 25 May 2021; Accepted 28 June 2021
Available online 8 July 2021

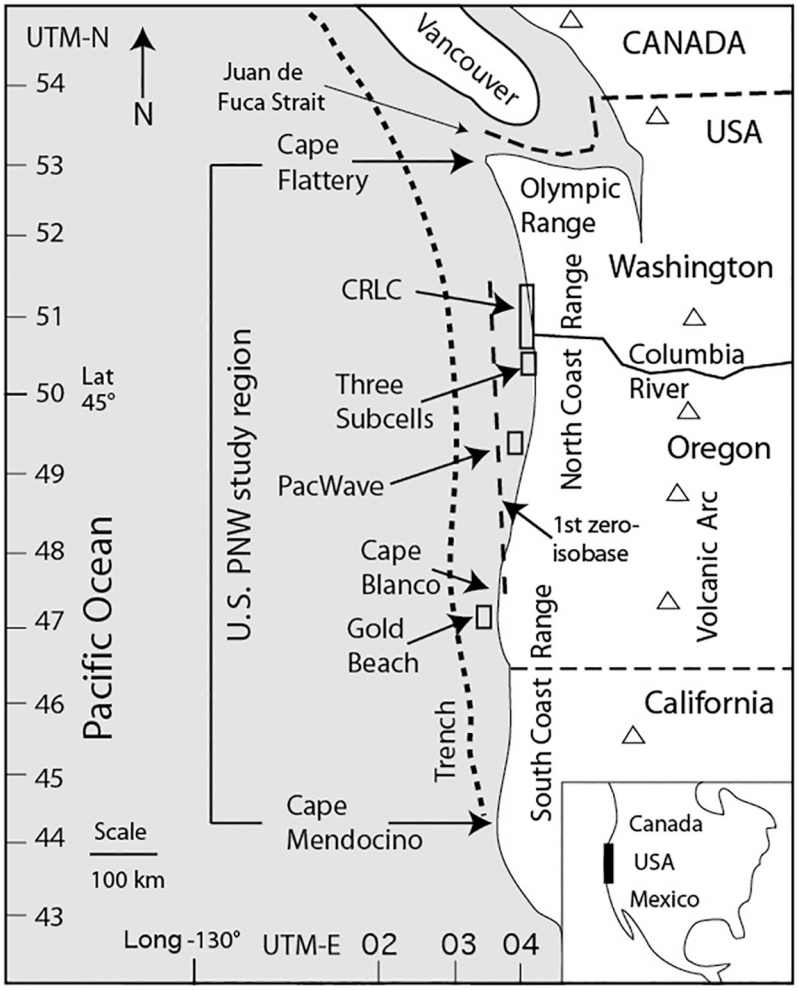

Fig. 1. Map of U.S. PNW coastal region. The U.S. PNW study region is bounded by Cape Flattery to the north and Cape Mendocino to the south. Four study areas analyzed for littoral sand displacements to submarine accommodation spaces include 1) Cape Blanco-Gold Beach (Clifton et al., 1991), 2) the Columbia River Littoral Cell (CRLC) (Peterson et al., 2020a), the Three Subcells (Peterson et al., 2020b), and the Pacific Wave Energy (PacWave) study area (PacWave, 2019). The central and southern parts of the Cascadia subduction zone extend landward from the buried trench (Trench). The Cascade volcanic range is shown by volcanoes (open triangles). Three uplifted coastal ranges include the Olympic Range and the North and South Coastal Ranges. Mega-folding of the upper-plate (landward of the trench) causes cyclic regional interseismic uplift and coseismic subsidence (0.5–2.0 m) landward of the 1st zero-isobase (Peterson et al., 2000; Peterson et al., 2012). (For interpretation of the references to colour in this figure legend, the reader is referred to the web version of this article.)

(CRLC) system. In this article, the PNW subcells refer to semi-contiguous beaches that are divided by seaward projecting headlands, which partially restrict alongshore transport over century time scales (Peterson et al., 1991, 2009, 2020b). All of the PNW subcells share in high-wave energies (peak $H_s \geq 10$ m), meso-tidal ranges (~3 m), and onshore wind forcing (sustained winds ≥ 8 m s^{-1}). Many of the sandy beaches in the PNW study region demonstrate susceptibilities to beach sand erosion from increasing accommodation spaces in the inner-shelf during latest-Holocene conditions of SLR (1.0 m ka^{-1}) (Peterson et al., 2019). Those increases could accelerate by 10× in the near future due to predicted increases in the rates of global SLR (up to 1.0 m 100 yr^{-1}). The responses of the different PNW littoral cell systems to corresponding increases in offshore and inshore submarine accommodation spaces are the subjects of this article. Such submarine accommodation spaces occur in the inner-shelf and in marine-dominated estuaries, as explained below in Background sections 2.2 and 2.3.

Evaluations of potential beach sand losses for given SLR scenarios require area-specific knowledge about 1) the conditions of existing beach sand reserves, 2) new sand supplies from rivers or alongshore transport, and 3) the magnitudes of competing submarine accommodation spaces for littoral sand in the inner-shelf, estuaries, and lagoons (Wilcoxen, 1986; Bruun, 1988; Shaw et al., 1998; Zhang et al., 2004; Stive, 2004; Davidson-Arnott, 2005; Brunel and Sabatier, 2009; Masselink and Russell, 2013; Toimil et al., 2017; Vousdoukas et al., 2020). Some of the beaches in the central PNW region were evaluated for potential retreat following great earthquake subsidence events (1 ± 0.5 m abrupt subsidence) using shifted equilibrium-profile methods (Doyle, 1996). Estimated retreats of ~100 m for 1.0 m of SLR would eliminate some of the narrower beaches (≤100 m width) in the region (Peterson et al., 2000). However, these methods did not account for shallow wave-cut 'bedrock' platforms, river sand supply, estuary sand sinks, or potential longshore transport within some subcells. Such conditions have been addressed, using accommodation space approaches, in one large littoral system, the Columbia River Littoral Cell (CRLC) (Peterson et al., 2020a) and in three small littoral subcells in the adjacent Three Subcells study area (Peterson et al., 2020b), but not along the remainder (80%) of the PNW coastline (Fig. 1). In this article, data from 1) heavy-mineral analyses of beach sand sources, 2) river sand supply, 3) estuarine littoral sand sinks, 4) existing beach sand volumes, and 5) potential inner-shelf sand sinks are compiled for contiguous beach segments (5–88 km in length) in the PNW coast. These data are analyzed at the subcell scale to estimate beach sand volume loss from 0.5 and 1.0 m values of SLR during the next century, assuming century time-scale beach equilibrium with the submarine accommodation spaces. The factors that lead to predicted beach sand volume losses are identified, as well as regional distributions of subcells that are most at-risk to near-future SLR. Most importantly, this article establishes the case for catastrophic erosion of nearly all of the existing PNW active-beaches (90% by length) from a potential SLR of 1.0 m during the next century. The loss of the current active-beaches could result in erosional beach step backs in natural soft sand shorelines or a complete loss of beach sand in front of indurated sea cliffs and artificially hardened shorelines. The use of submarine accommodation space methods to evaluate beach sand erosion over the wide range of beach conditions in the PNW region should have broad application to many other complex sandy shorelines in high-energy open-ocean coastlines around the world.

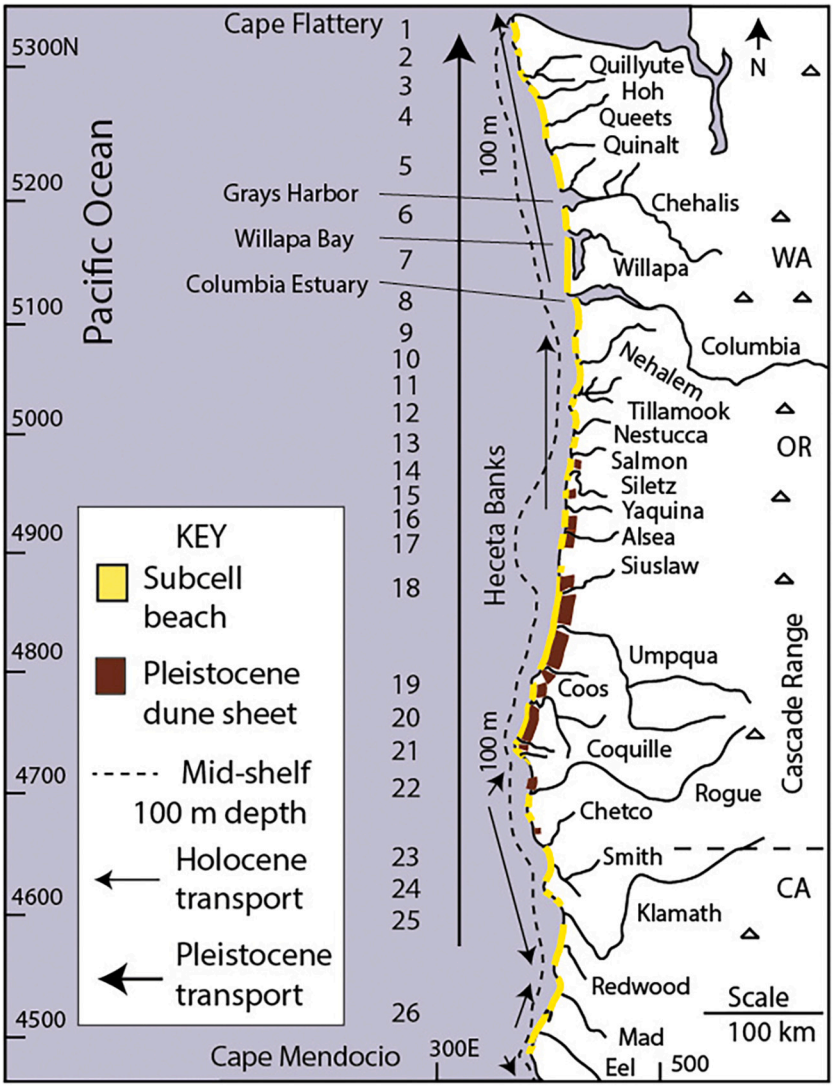

Fig. 2. Map of subcell beaches in the U.S. PNW study region. Map shows 34 littoral subcell beaches (yellow lines) of at least ~5 km in length, including 26 subcells (numbered 1–26) that have been surveyed for beach sand volume (Table 1). Latest-Pleistocene dune sheet remnants (brown lines) are distributed north and south of a major shelf bight (Heceta Banks), as outlined by the mid-shelf bathymetric contour (−100 m dashed line). Large antecedent rivers, including the Columbia, Umpqua, Rogue and Klamath Rivers are shown reaching the Cascade volcanic arc (triangles). Smaller rivers (named) drain the Coast Ranges (Fig. 1). Three large estuaries (Columbia River Estuary, Willapa Bay, and Grays Harbor) divide, but do not isolate, four subcells in the CRLC system. Late-Holocene littoral transport directions are shown (arrows) with net-northward transport transitioning to generally net-southward transport, respectively, in the north and south ends of the PNW study region. Two anomalous reversals of net southward littoral transport occur north of the Eel and Rogue Rivers, due to a northeast shoreline-alignments (Bodin, 1982; Peterson et al., 2009). Late-Pleistocene littoral transport along what is presently the mid-shelf was dominantly northward throughout the entire PNW study region during marine low-stand conditions (Scheidegger et al., 1971; Venkatarathnam and McManus, 1973; Peterson et al., 2007). Map coordinates are in UTM 10 N positions (km). (For interpretation of the references to colour in this figure legend, the reader is referred to the web version of this article.)

2. Background

2.1. U.S. PNW coastal geomorphology

The U.S. PNW coastline (~1000 km in distance) contains 34 semi-contiguous sandy beaches of at least ~5 km in length, which total ~ 700 km in combined length (Fig. 2; Table 1) (Peterson et al., 1991). Mean grain sizes of representative beach sand samples in the PNW region range from 0.10 mm to 3.71 mm, and average 0.35 ± 0.37 mm 1σ (n = 201) (Peterson et al., 1994). Contiguous beach shorelines range from 4.5 km to 88.0 km in alongshore length. They are generally developed in north-south orientations, though locally variable neotectonic uplift between Cape Blanco and Cape Mendocino (Fig. 1) has aligned several shorelines by as much as 30° from the general north-south trend (Bodin, 1982; Muhs et al., 1990). The contiguous beaches are bounded between resistant bedrock headlands (0.1–3.5 km seaward projections). The smaller headlands (<0.5 m seaward projection distances) likely permit littoral sand bypassing between the subcells at interdecadal time scales (Peterson et al., 2020b). The time scales of sand bypassing around the largest headlands (>1.5 km seaward projections) are not established. Alongshore transport within the subcells reverses seasonally, through net-northward and net-southward transport, respectively, occur in the northern and southern ends of the PNW region (Peterson et al., 2009). Averaged beach widths within corresponding subcells range from 30 m to 270 m in across-shore distance, as measured by aerial photography and satellite imagery. The largest beach widths are associated with abundant littoral sand supply from the very-large Columbia River, ~2.2 × 10^6 m^3 yr^{-1} bedload, as estimated from Karlin (1980). The narrowest beaches are generally associated with small pocket beaches that lack direct river sand supply and/or are isolated from adjacent subcells by large headlands. The smaller subcells without direct river sand supply likely receive some sand from sea cliff erosion, but not in sufficient abundance to produce wide beaches (>100 m in width). Erosion of unconsolidated dune/ramp sand deposits in retreating sea cliffs previously supplied some PNW subcells with substantial sand volumes (~0.4 × 10^6 m^3–3.4 × 10^6 m^3 for 15° paleo-ramp slopes) during latest-Holocene time (Peterson et al., 2019). Glacial outwash deposit terraces have similarly supplied small pocket beaches in the northernmost PNW region (Swartz et al., 1985; Peterson et al., 2014a). However, most of those unconsolidated sand ramps, uplifted marine terraces, and outwash terrace reserves are now gone, as the remaining unconsolidated deposits are perched above low bedrock platforms/sea cliffs (~20% of the coastline) (Peterson et al., 1994). Higher-bedrock sea cliffs in the central and southern PNW region (~20% of the coastline) are composed of indurated mudstones and lithified sandstones, volcanic rocks, or metamorphic rocks, which are resistant to surf erosion over short (one century) time scales. Barrier spits, beach plains, and dune deflation plains account for ~40% of the PNW coastline (Peterson et al.,

Table 1
Littoral subcell parameters in the PNW region.

Subcell	UTM-N (m) north-south	Subcell length (km)	Headland projections (km)	River sand sources	Estuary sand sinks	Beach widths m ± 1σ (m)
Hobuck (1)	5,355,200–5,350,750	7.0	n1.1, s1.1	–	–	150 ± 70
Shi Shi (2)	5,348,959–5,344,950	4.5	n0.7, s0.5	–	–	70 ± 50
Sand Pt	5,331,550–5,328,750	4.5	n0.4, s0.5	–		80 ± 70
La Push (3)	5,310,950–5,304,300	6.6	n0.4, s0.7	Quillyute	–	80 ± 50
Kalaloch (4)	5,304,000–5,251,250	56.7	n0.7, s0.2	Hoh, Queets	–	60 ± 40
North Beach (5)	5,239,650–5,197,900	43.0	n0.6, –	Columbia	Grays Harbor	270 ± 90
Grayland (6)	5,194,950–5,176,250	18.3	–	Columbia	Grays Harbor	250 ± 60
Long Beach (7)	5,165,800–5,124,150	43.7	–	Columbia	Willapa Bay	200 ± 80
Clatsop (8)	5,119,200–5,091,700	28.8	-, s2.5	Columbia	–	210 ± 60
Cannon (9)	5,084,150–5,070,000	14.5	n2.5, s1.1	–	–	80 ± 40
Tillamook (10)	5,064,450–5,038,100	25.5	n1.3, s0.7	Nehalem, Wilson	Nehalem, Tillamook	140 ± 50
Netarts (11)	5,036,800–5,022,850	14.5	n0.6, s2.5	–	Netarts	110 ± 70
Sand Lake (12)	5,020,800–5,008,000	12.5	n2.6, s0.6	Nestucca	Nestucca	140 ± 70
Pacific City (13)	5,007,400–4,994,100	13.0	n0.6, s1.3			120 ± 50
Lincoln City (14)	4,986,150–4,965,350	21.0	n0.4, s0.7	Siletz, Salmon	Siletz, Salmon	80 ± 40
Otter Rock (15)	4,955,400–4,947,600	8.0	n1.5, s0.9	–	–	80 ± 30
Newport (16)	4,947,100–4,927,800	19.5	n1.5, s0.2	Yaquina	Yaquina	80 ± 40
Waldport (17)	4,926,000–4,909,150	17.0	n0.2, s0.4	Alsea	Alsea	80 ± 40
Big Creek	4,894,850–4,888,350	6.5	n0.2, s0.5	–	–	70 ± 50
Winchester (18)	4,884,300–4,799,150	88.0	n0.4, s0.8	Siuslaw, Coos, Umpqua	Siuslaw, Coos, Umpqua	90 ± 40
Bullards (19)	4,791,800–4,773,350	18.5	n2.5, s0.3	Coquille		160 ± 60
Bandon (20)	4,773,350–4,748,550	26.5	n0.3, s0.5	Coquille	–	130 ± 70
Sixes	4,747,400–4,743,800	4.5	n0.6, s1.0	Sixes	–	40 ± 20
Garrison (21)	4,743,400–4,732,900	11.0	n0.6, s0.4	Elk	–	60 ± 40
Port Orford	4,732,800–4,727,050	8.0	n2.0, s0.8	–	–	40 ± 40
Nesika	4,714,650–4,705,900	9.0	n1.1, s0.1	Rogue	–	60 ± 30
Gold Beach (22)	4,702,000–4,688,650	13.5	n0.5, s0.3	Rogue	–	70 ± 30
Pistol	4,686,000–4,678,800	7.5	n0.7, s0.3	Pistol	–	70 ± 30
Brookings (23)	4,655,450–4,626,500	33.0	n1.6, s0.6	Chetco, Smith Winchuck Ck	–	50 ± 20
N. Crescent	4,626,000–4,622,000	5.0	n0.8, s0.2	–	–	30 ± 30
S. Crescent (24)	4,622,000–4,617,000	5.0	n1.6, s0.2	–	–	40 ± 30
Orick (25)	4,600,000–4,554,900	46.0	n1.2, s1.4	Klamath, Redwood Ck	–	60 ± 20
Eureka (26)	4,542,700–4,485,700	65.5	n3.5, s0.3	Mad, Eel	Humboldt	70 ± 40
Mendocino	4,484,400–4,478,200	6.5	n0.7, s0.3	Eel	–	50 ± 30

Notes: Subcells are identified by name. Subcells surveyed for existing beach volumes are identified by number (1–26). Beach terminations (north-south) are shown by UTM-N (m) coordinates. Subcell alongshore lengths (km) are based on bounding (dividing) headlands. North (n) and south (s) headland seaward projections (km) are taken seaward from adjacent beach segments (Peterson et al., 1994; Peterson et al., 2009). Subcell river sand sources, estuary sand sinks, and averaged beach widths (mean ± 1σ m) are from Peterson et al. (1994). The active-beach widths were measured from mid-swash runups on the beach faces to the sea cliffs or seaward edge of foredune vegetation at 0.5 km alongshore intervals (low elevation aerial photo/video), then averaged for each subcell (Rosenfeld et al., 1991). The four subcells in the Columbia River Littoral Cell (CRLC) are divided, but not isolated, by large tidal inlets of the Columbia River, Willapa Bay, and Grays Harbor (Chehalis) estuaries (Fig. 2). Numbered subcells (1–26) were surveyed (profiled) and subsurface-tested for existing beach sand volumes (Pettit, 1990; Peterson et al., 1994; Doyle, 1996; Percy et al., 1998; Vanderburgh et al., 2003; Vanderburgh et al., 2010).

1994). Therefore, potential new sources of beach sand from eroding sea cliffs are largely limited to semi-indurated late-Pleistocene dune sheet deposits and uplifted marine terrace deposits (~20% of the coastline) in the central PNW region (Fig. 2) (Baldwin et al., 1973; Schlicker et al., 1973; Peterson et al., 1994). Projected accelerations of modern erosion rates of the late-Pleistocene semi-indurated sandy deposits in uplifted marine terraces (5–30 m elevation) of the central Oregon coast (Priest, 1999; Peterson et al., 2006) might not be sufficient to significantly offset estimated beach erosion during the next century, as discussed below in Section 5.1. However, the nonindurated (uncemented) Holocene sand deposits in the larger active sand ramps and bay spits (Peterson et al., 2019) are included in the analyses of back-beach erosion contributions to near-future beach sand supply (see Discussion Section 5.3).

In the northern Oregon and Washington coasts (Fig. 1), regional coseismic subsidence events (0.5–2.0 m of abrupt relative sea level rise) alternate with intervals of interseismic uplift, with recurrence intervals of 200–800 years (Darienzo and Peterson, 1990; Atwater et al., 2003). The last Cascadia megathrust rupture and corresponding tsunami excitation occurred in 1700 CE (Satake et al., 1996). Due to an apparent coastal crossing of the 1st zero-isobase in south-central Oregon, only the northern part of the PNW Cascadia margin experiences substantial regional coseismic subsidence (>0.5 m) (Peterson et al., 2012). However, a coseismic subsidence event of 1–2 m in the north-central part of the PNW region (Doyle, 1996; Barnett, 1997; Peterson et al., 2000) could locally equal or double the currently predicted upper-limit (1.0 m) of eustatic (global) SLR in the next century. Modern interseismic vertical displacements of the PNW coast generally range from −1 to +3 mm yr^{-1} (Cruikshank and Peterson, 2017). At present, an average displacement of +1.8 mm yr^{-1} is calculated for the PNW coastal region. Modern eustatic SLR (~2.5 mm yr^{-1}) offsets the regionally averaged displacement to yield an averaged net SLR rate of 0.7 mm yr^{-1} for the PNW region. Over a one century period that rate would yield a 7 cm net SLR. For this article we assume potential SLR values of 50 and 100 cm for the next century. Those values represent SLR rates some 7–15 times greater than the current averaged SLR rate in the PNW region.

Pacific Northwest beaches have been studied for short and long-term responses to sea level changes. At the shortest time scales (intra-annual) some beaches can erode by up to 100 m from major winter wave- and wind-storm surges (~1 m height), but return to fair weather profiles during spring, summer, and fall months. At moderate time scales (decades), the progradational beaches of the CRLC system, in the central Cascadia subduction zone (Fig. 1) respond to abrupt coseismic subsidence (1–2 m) with large retreat scarps (~ 10 m in height) (Meyers et al., 1996; Peterson et al., 2010; Peterson et al., 2020a). The beaches develop

Table 2
River and estuary sediment sources and compositions.

River/ estuary*	UTM-N (m)	Tributary suspended load ($\times 10^3$ t yr^{-1})	Tributary bedload ($\times 10^3$ m^3 yr^1)	Estuary MTL area (km^2)	Estuary MLW area (km^2)	Estuary bMTL sand fraction (%)	Estuary bMTL beach sand (%)	Ref
Quillayute	5307100	204	31					
Hoh	5289400	82	13					
Queets	5266600	144	22					
Quinault	5244600	86	13					
Chehalis/ GH*	5196500	665	101	203	116	70	60	1, 2
Willapa Bay*	5169000	131	20	252	158	80	95	3
Columbia*	121500	14,282	2178	332	252	90	0	4, 5
Nehalem*	5056100	54	33	6.75	3.84	50	10	6
Tillamook*	5046300	44	27	25.12	16.7	50	20	6
Netarts*	5031900	–	–	6.35	3.29	90	100	6
Sand Lake*	5013850	–	–	1.33	0.53	90	100	7
Nestucca*	5000900	58	9	2.88	1.71	90	20	7
Salmon*	988500	24	4	0.57	0.3	100	20	2
Siletz*	4975200	65	10	3.23	1.67	80	30	2
Yaquina*	4940500	84	13	13.08	10.35	70	40	8
Alsea*	4919200	162	25	6.71	4.73	90	30	2
Siuslaw*	4874200	190	29	7.55	6.03	95	40	2
Umpqua*	4835600	3243	495	24.5	21.44	80	10	9
Coos*	4800850	196	30	33.35	23.51	70	50	10, 11
Coquille	4775000	245	37					
Sixes	4745700	358	55					
Elk	697300	85	13					
Rogue	4697300	4688	715					
Pistol	4680500	96	15					
Chetco	655250	246	37					
Winchuck	651000	70	11					
Smith	4644400	552	84					
Klamath	4599100	10,877	1659					
Mad	535200	2518	384					
Humboldt*	512500	lagoon	–	45.18	27.97	25	100	12
Eel	4499400	24,751	3774					

Notes: Rivers with estuaries and lagoons (*) are included here, based on significant tidal areas relative to fluvial discharge (Peterson et al., 1991). The Chehalis River tributaries drain into the Grays Harbor (GH) estuary. River, estuary, and lagoon positions are shown as river mouth or tidal inlet UTM northing positions (m). Drainage basin annual bedload discharge ($\times 10^3$ m^3 yr^{-1}) is estimated from drainage basin suspended sediment discharge ($\times 10^3$ tons yr^{-1}) (Karlin, 1980), assuming bedload is 25% of the suspended load fraction and a bedload sand mass to sand volume conversion ratio of 0.61. Tidal level surface areas (km^2) are from Percy et al. (1974), with the exception of Humboldt Bay (Barnhart et al., 1992). Estuary surface deposit sediment compositions below mean tidal level (bMTL) are based on reported studies (Ref) as follows: (1) Barrick (1976), (2) Peterson et al. (1984), (3) Peterson and Vanderburgh (2018a), (4) CREDDP (1983), (5) Peterson et al. (2014a, 2014b), (6) Peterson et al. (2020b), (7) proxy data from a similar adjacent estuary/lagoon (Netarts- > Sand Lake; Salmon- > Nestucca), (8) Kulm and Byrne (1966), (9) Briggs and Peterson, 1995), (10) Arneson (1975), (11) Baker (1978), (12) Jones (2015). See Table 1 for hosting subcells. See Fig. 2 for river/estuary locations.

progradational profiles following interseismic uplift (~100 years) and the associated return of the displaced (offshore) sand supply. Net progradations occur during prolonged interseismic stable intervals (multi-century) due to abundant Columbia River sand supply, which preserves the episodic catastrophic beach erosion records throughout the CRLC system. The responses of the CRLC shorelines to coseismic subsidence events provide constraints on the time scales of beach sand displacements to inner-shelf settings and large estuaries in the PNW region (Peterson et al., 2020a), as explained in Section 2.3 below.

Many of the narrower beaches located south of the CRLC in northern Oregon (Fig. 1; Table 1) are ^{14}C dated by underlying beach platform stumps (Hart and Peterson, 2007) or paleo-sand ramps (Peterson et al., 2019) to several thousands of years in age. The beach platform stumps are thought to have initially derived from neotectonic cycles of coseismic subsidence that episodically erode platforms and interseismic uplift that raise the platforms above the reach of winter storm surges, leading to forest colonization. The impermeable bedrock platforms would have suppressed subsurface salinity intrusion and upheld freshwater discharge from adjacent sea cliffs and creeks, encouraging forest colonization of the narrow uplifted platforms. Under local conditions of excess beach sand supply, from rivers, the inner-shelf, eroding sea cliffs, and/or longshore redistributions some of the beaches accumulated sufficient sand during long interseismic cycles to bury the platform trees and intact forest soils (Hart and Peterson, 2007). The forest burial by beach sand and/or eolian sand ramp deposits thereby protected the buried stumps from subsequent coseismic subsidence events and/or net SLR (1.0 m ka^{-1}) in latest-Holocene time. Over historic time scales, some of the protective beach deposits appear to be in dynamic equilibrium with seasonally varying wave and sand supply conditions. However, over millennial time scales, many of the narrower beaches show evidence of gradually declining sand supply, as based on the progressive erosion of the beach platform stumps and the basal truncation of paleo-sand ramps (Peterson et al., 2019). Beach sand supply from local sea cliff erosion has not kept pace with latest-Holocene SLR and/or longshore transport in the narrowest beaches (< 50 m width) of northern Washington and southern Oregon (Peterson et al., 1994) (Table 1), even where large active landslides occur (Kingen, 2021). Although mineralogical analyses show significant inputs of late-Pleistocene dune sheet sand to the wider beaches (80–140 m widths) in central Oregon (Table 1) (Peterson et al., 2020b) it is not known to what extent modern sea cliff erosion contributes to modern beach sand supply in those wider beaches. The regional gradual losses of beach sand in subcells without large rivers in latest-Holocene time (3–0 ka) are attributed to increasing accommodation spaces for littoral sand in the submarine settings of the innermost-shelf and estuaries. Such submarine accommodation space increases resulted from the net SLR (1.0 m ka^{-1}) in latest-Holocene time (Peterson et al., 2019). In this article, it is presumed that a near-future increase in the rate of SLR would increase the submarine accommodation space volumes, thereby shifting the apparent equilibriums in beach sand supplies to the offshore (inner-shelf) and inshore (estuary)

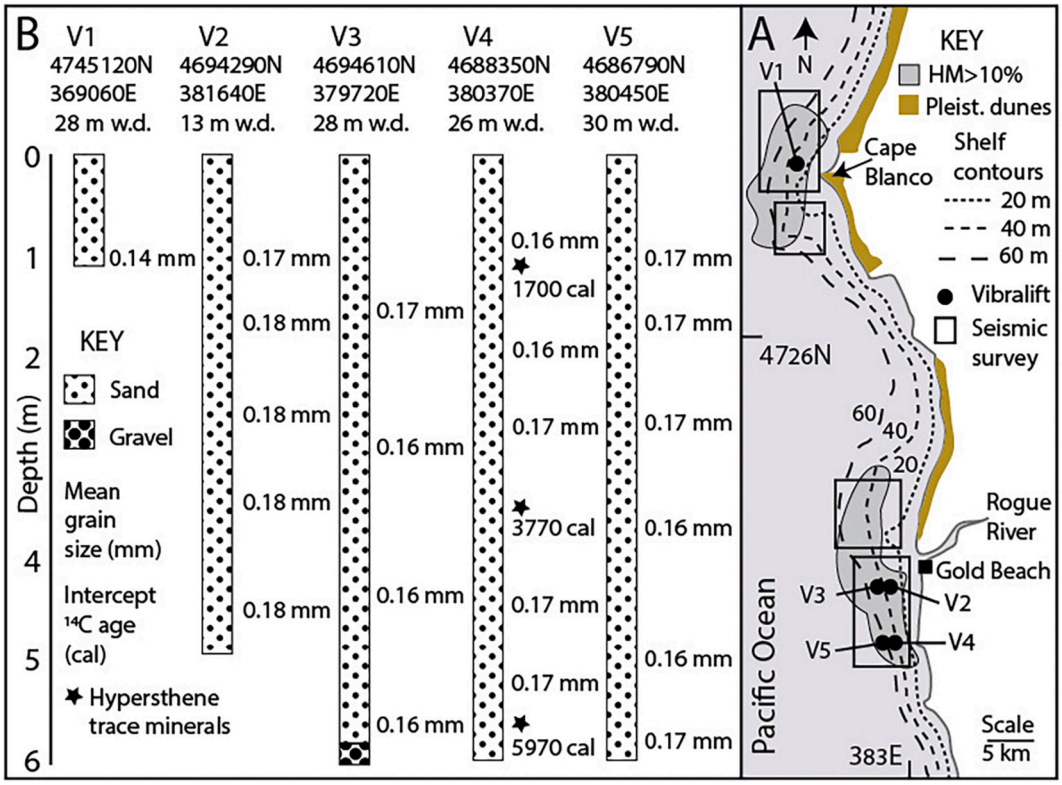

Fig. 3. Inner-shelf sedimentation in Southern Oregon. Part A (map) shows 1) onshore distributions of late-Pleistocene dune sheets (Peterson et al., 2007), 2) inner-shelf bathymetric contours, 3) heavy-mineral (HM) anomalies in surface deposits at Cape Blanco and Gold Beach, Oregon (shaded) (Kulm and Peterson, 1990), 4) seismic survey areas (boxes), and 5) vibralift stations (V1–5) (solid circles) (Clifton et al., 1991). Part B (stratigraphic columns) shows 1) vibralift station locations in meters (UTM 10-N), water depth (w.d.) in meters (m), 3) sediment texture (well-sorted sand or gravel), 4) sieved sand mean grain size (mm) (Mardock, 1991), 5) heavy-mineral fractions enriched in hypersthene (tracer mineral for Rogue River sand supply) (Scheidegger et al., 1971), and 6) calibrated ^{14}C intercept ages of marine shells in years BP (cal) (Clifton et al., 1991). The locations of the Cape Blanco and Gold Beach Oregon, in the Southern Oregon Coast are shown in Fig. 1. (For interpretation of the references to colour in this figure legend, the reader is referred to the web version of this article.)

depositional settings in the PNW region (Peterson et al., 2020a, 2020b). Estimates of these littoral sand displacements are used in this study to predict near future conditions of beach erosion in the PNW study region.

2.2. Rives and estuaries in the PNW region

Latest-Holocene sediment supplies and submarine accommodation spaces have been previously reported for some PNW estuaries and their associated tributaries, including the Columbia River estuary, Willapa Bay, and Grays Harbor estuary in the CRLC (Peterson et al., 2020a), and the Tillamook, Nehalem, and Netarts Bays in the Three Subcells study area (Fig. 1) (Peterson et al., 2020b). Historic sediment discharge from all of the larger tributary drainages (Karlin, 1980) and surface deposit compositions in the smaller estuaries are compiled in Table 2. Annual river bedload-discharge values range widely (4×10^3 -to- 3774×10^3 m^3 yr^{-1}) between the different tributary systems. The annual bedload discharge volumes from the tributaries are multiplied by 100 years duration in Discussion Section 5.1 to estimate river sand supply to the subcell beaches, during the assumed one century period of near-future SLR. Assuming potentials of 0.5–1.0 m of near-future SLR, only the estuary surface areas in the subtidal and lower intertidal levels are expected to accumulate significant river or beach sand, as the upper-intertidal levels in the PNW estuaries generally accumulate mud (Peterson and Vanderburgh, 2018a, 2018b; Peterson et al., 2020b). For the purposes of this study, the surface sediment compositions of the estuaries are averaged on the bases of combined surface areas below the mean tidal level (MTL) (Table 2). Those data are used later in Discussion Section 5.1 to estimate accommodation space increases or volume accumulations of river sand and beach sand in the estuaries and lagoons relative to potential near-future SLR.

2.3. Seaward dispersal and deposition of littoral sand across the innermost-shelf

During the mid-1980s, a task force was formed to study the potential for economic heavy-mineral placers in the southern Oregon continental shelf at Gold Beach (Fig. 1) (Clifton et al., 1990). Seismic reflection surveys in the Cape Blanco and Gold Beach survey areas (Fig. 3) demonstrated that undeformed latest-Quaternary sediments in the inner-shelf ranged from 0 to 30 m in thickness and averaged 10 m in thickness (Clifton et al., 1991). Ground-truthing by vibralift sampling in the Gold Beach study area (water depths 13 to 30 m) showed that the uppermost 5–6 m of the innermost-shelf deposits are dominated by unconsolidated fine sand (0.14–0.18 mm sieved diameter). No increased concentrations of heavy minerals (placers) occurred at depth in any of the vibralift stations (Mardock, 1991). The weak and diffuse heavy-mineral anomalies in surface samples from the inner-shelf reflect 1) heavy-mineral lags offshore of river mouths and/or 2) winnowing processes by shelf bottom currents. Such bottom currents, presumably including combined oscillatory and unidirectional flows, are interpreted to be locally intensified around headlands, offshore shoals, and changing bathymetric contour orientations. Gravel was only encountered in one vibralift sample, which was collected from the base of a six meter-depth section at station V3. A lack of cemented sand, loess layers, or soil concretions in any of the vibralift samples, ruled out penetration into underlying latest-Pleistocene dune sheet deposits. Such dune sheets had crossed the inner-shelf during marine low-stand conditions to supply the landward dune sheet remnants, as shown in Fig. 3 (Peterson et al.,

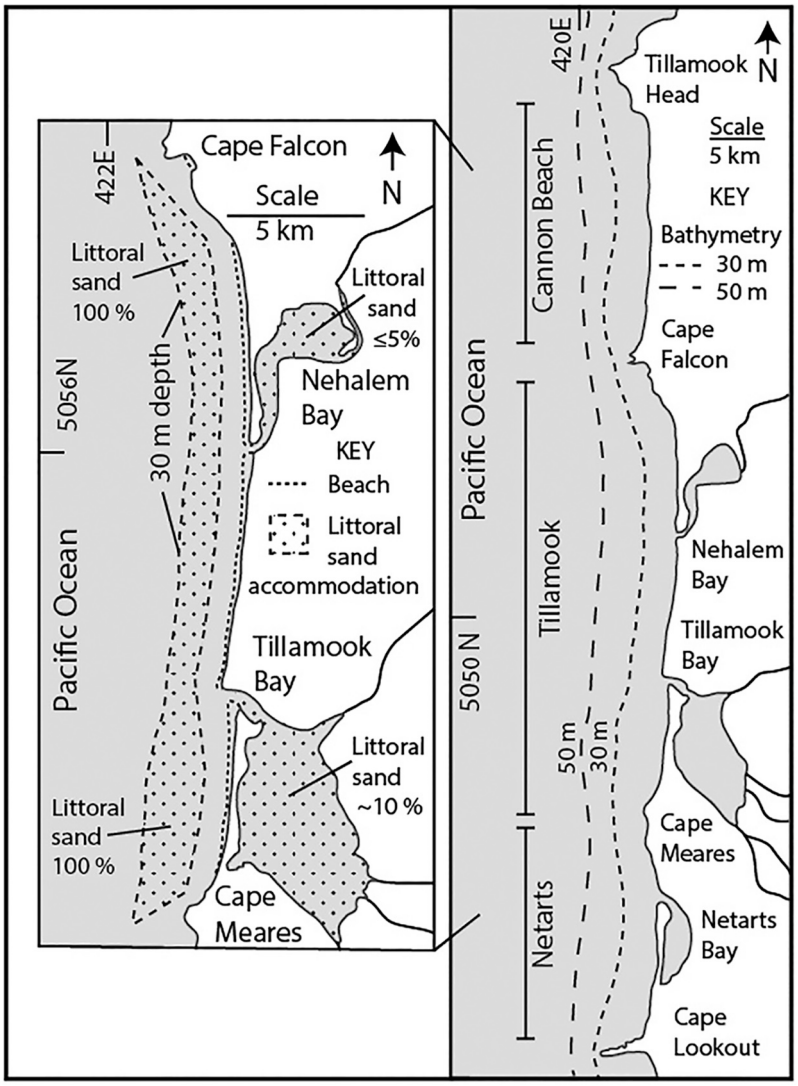

Fig. 4. Submarine accommodation spaces in three small subcells in northern Oregon. Three small subcells in the Three Subcells study area of northern Oregon (Peterson et al., 2020b) were evaluated for potential beach sand volume loss, following potential SLR or vertical sand accretion in submarine accommodation spaces. The submarine accommodation spaces include the innermost-shelf to at least 30 m water depth (−30 m bathymetric elevation) and small estuaries. One subcell, Tillamook, is enlarged (inset) to show details of 1) offshore accommodation space (100% littoral sand) in the innermost-shelf between 30 m water depth and a transition zone (~1.0 km offshore of the modern shoreline) and 2) estuarine sand accommodation spaces in Tillamook and Nehalem Bays. Modern deposits below mean tidal level (MTL) in Tillamook Bay are ~50% sand fractions, of which ~20% are from beach sand sources, thereby yielding ~10% littoral sand accommodation space, in proportion to MTL surface area in Tillamook Bay. Maps are redrafted from Peterson et al. (2020b).

2007). Vibralift station V4 was selected for heavy-mineral analysis and ^{14}C dating of shell fragments in the recovered sand section (1–6 m depth subsurface) (Clifton et al., 1991). Sand and shell fragments were sampled from the bottoms of discrete drives to reduce bias from sediment mixing during coring. Dated samples have the following radiocarbon ages: ~1.0 m depth, marine calibrated 1520–1890 2σ, intercept 1700 (Beta-45,569); 3.7 m depth, marine calibrated 3580–3960 2σ, intercept 3770 (Beta-45,570); and 6.1 m depth, marine calibrated 5740–6120 2σ, intercept 5970 (Beta-45,571) (Calib7.10, 2020). The intermediate sample at 3.7 m subsurface depth, and a corresponding 3770 intercept age, yield a sand sedimentation rate of 1.0 m ka^{-1}, during latest-Holocene time. Heavy-mineral analyses of three sand samples from vibralift station V4 demonstrated enriched hypersthene relative to augite (0.7–0.9), as shown in Results Section 4.2. The enriched hypersthene indicates significant contributions of sand supply from the nearby Rogue River (Scheidegger et al., 1971) but not the outer-shelf (see Results Section 4.2 for sand heavy-mineral analyses).

The composition of inner-shelf deposits, located offshore of the southern Oregon Coast (Fig. 3), demonstrate seaward dispersal and deposition of beach sand, as derived, in part, from local river sand supply during late-Holocene time. The offshore deposition of beach sand is thought to result from the infilling of increased accommodation space in the inner-shelf, following initial wave scour in mid-Holocene time and then sea bottom submergence from relative SLR in late-Holocene time (Peterson et al., 2019) (see Fig. 4 below). Similar results have been recently reported from a compilation of several studies (1994–2006) that were conducted in the large Columbia River Littoral Cell (CRLC) in northernmost Oregon and southern Washington (Fig. 1) (Peterson et al., 2020a). The large CRLC system (160 km in length) is abundantly supplied with littoral sand from the Columbia River. Extensive offshore vibracore sampling in the CRLC inner-shelf (n = 30 ^{14}C-dated vibracores) demonstrated that vertical accretion of beach sand, as supplied by the Columbia River, in the inner-shelf (10–40 m water depth) kept pace with, or exceeded, latest-Holocene SLR (1.0 m ka^{-1}). Net accumulation occurred where the seaward-slope gradients of the inner-shelf equaled or exceeded 0.40%. The broad inner-shelf and large estuary sinks of beach sand in the CRLC system are estimated to yield catastrophic barrier and beach plain shoreline retreat distances (~0.3–1.5 km) from potential future SLR (1–3 m) during the next several centuries (Peterson et al., 2020a). Such retreat distances could erode 25–50% of the wide barrier spits and beach plains, generally 1–3 km in width in the CRL system. It is uncertain how future modifications of sediment flux near the mouth of the Columbia River might impact future beach retreat. Ruggiero et al. (2016) used cross-shore profiles (1997–2014) to document subtidal sand bars moving offshore and intertidal bars moving onshore to feed modern beach progradation in subcells located adjacent to the Columbia River mouth. It was not reported whether or how the bar migrations could have been influenced by 1) throughput of

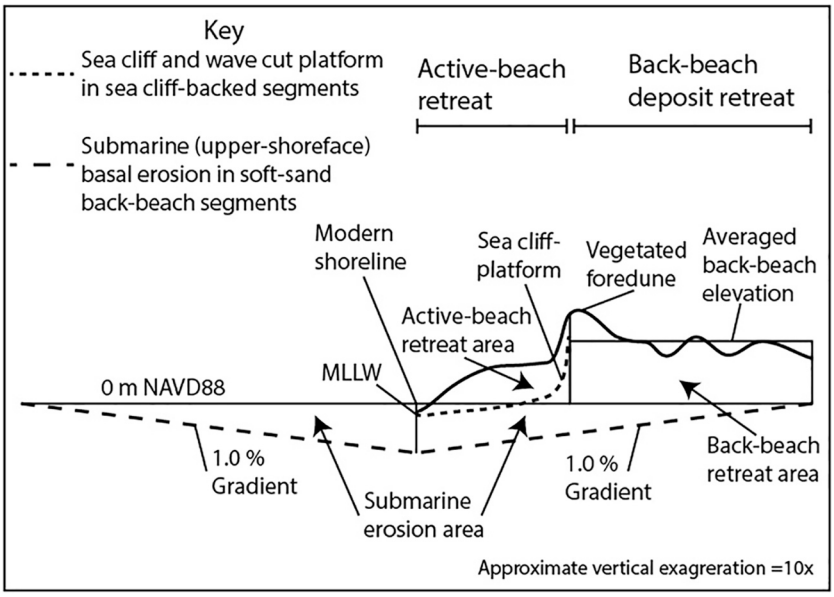

Fig. 5. Estimated beach retreats following potential near-future SLR. Plotted beach retreat cross-sections are based on estimated beach sand losses in 1) sea cliff backed-beaches (active-beach area retreats) and 2) soft-sand backed-beaches (active-beach and back-beach area retreats). The soft-sand backed-beach retreats include submarine erosion areas (Peterson et al., 2020a), whereas the sea-cliff backed beach retreats only include the active-beach areas above wave-cut platforms (bedrock) or the Mean Lower Low Water (MLLW) elevation (Peterson et al., 2020b). The landward gradient of basal submarine erosion (1.0%) is taken from the modern nearshore gradient in the CRLC or the innermost-shelf gradient for the other PNW subcells. An equivalent seaward gradient is used to taper-up to the transition zone of no net erosion in the offshore upper-shoreface (Bruun, 1962; Peterson et al., 2020a). The figure is redrafted (combined) from figures in Peterson et al. (2020a, 2020b).

Columbia River sand, 2) historic alterations of the Columbia River ebbtide delta (Ruggiero et al., 2016) and/or 3) recent changes in dredge spoil disposals from deep water to shallow water sites, as located offshore of the Columbia River mouth, after 1998 (USACE, 2005a). The widely-prograded barriers and beach plains in the large CRLC system are anomalous in the Pacific Northwest region. Most of the other beaches in the PNW region are narrow (30–160 m in width) (Table 1), fronting either sea cliffs, or receding/deflating foredune plains (Peterson et al., 1994). Such narrow beaches are thought to be susceptible to much smaller increases in potential near-future SLR (0.5–1.0 m), as summarized below.

2.4. Estimated sand volume loss following potential SLR in three Small Subcells

Three small subcells in the Three Subcells study area in northern Oregon (Fig. 1) were evaluated for estimated beach sand displacements to submarine accommodation spaces in the innermost-shelf (to 30 m water depth) and in small estuaries/lagoons, following potential near-future SLR (Fig. 4) (Peterson et al., 2020b). The narrow beaches (80–140 m in across-shore widths) in the Three Subcells study area are backed by either 1) sea cliffs (hard back-beach areas) or 2) receding foredunes and/or deflated dune-ridge beach plains or barrier spits (soft-sand back-beach areas). The small subcells record evidence of gradual sand loss from the beaches in latest-Holocene and historic times. The sand loss has been attributed to a net loss of beach sand reserves to the small estuaries and the inner-shelf during latest-Holocene conditions of net SLR and the corresponding increases in associated submarine accommodation spaces. The headland-bounded small subcells (14.5–25.5 km in length) are fronted by relatively steep inner-shelf gradients (1%), as shown by the inner-shelf bathymetric contours in Fig. 4. Most importantly, augite-enriched littoral sand was found to extend offshore from the modern beaches to more than 50 m water depth in all three subcells. Augite is supplied by the smaller rivers in the North Coast Range, and its presence indicates a component of beach sand supply from local rivers rather than from transgressive shelf sand sources. The augite-enriched inner-shelf sands thereby confirm offshore dispersal and net deposition of beach sand, derived, in part, from recent river sand supply, across the innermost-shelf in latest-Holocene time. The Three Subcells study area in northern Oregon differs from the adjacent large CRLC system in that it lacks a very-large river or tidal inlet ebb-tide deltas. The lack of a very-large river or ebb-tide deltas in the Three Subcells study area demonstrates the importance of ocean storm wind and wave processes (Sternberg, 1986; Kachel and Smith, 1986) in transporting the littoral sand out across the inner-shelf from the adjacent beaches in latest-Holocene time.

Evaluations of potential near-future beach erosion in the Three Subcells study area are based on assumed littoral sand vertical accretions (net sedimentation) of 0.5 m and 1.0 m thickness in submarine accommodation spaces, including the innermost-shelf and estuaries/lagoons (Fig. 4). These submarine accommodation spaces are expected to serve as beach sand sinks or repositories during the next century of predicted SLR (Peterson et al., 2020b). The computed sand sinks were then compared to the existing beach sand reserves to yield averaged beach sand volume deficits in each subcell. For those subcells with soft-sand back-beach areas (Fig. 5), the volume of potential sand loss (deficit) was used to calculate the back-beach retreat distance, beyond the eroded active-beach. Such soft-shorelines are assumed to include submarine erosion areas, as based on equilibrium profile shifts and measured catastrophic beach retreat scarps in the CRLC system (Peterson et al., 2020a). In summary, the potential filling of submarine accommodation spaces in each of the three subcells by 1.0 m of vertical sand accretion, primarily in the innermost-shelf, would eliminate all of the sea cliff-backed beaches and substantially erode the soft-sand back-beach areas by >150 m distance, or a total shoreline retreat (active-beach and back-beach) of >250 m distance in the Three Subcells study area.

3. Methods

The details and justifications of the methods used in this regional study have been previously described in Peterson et al. (2020a, 2020b). Summaries of the methods used here are outlined below. Comprehensive data tables compiled for this study are presented in Peterson and Kingen (2021). Those larger data sets are averaged and/or plotted in summary tables and figurers in the Results section of this article.

Heavy minerals are used as tracers for sand sources (river and remobilized shelf deposits) and sand sinks (inner-shelf and estuaries) in the PNW study region (Glenn, 1960; Scheidegger et al., 1971; Venkatarathnam and McManus, 1973; Scheidegger and Phipps, 1976; Peterson et al., 1984; Baker et al., 2010). Mono-mineralic colored pyroxenes (augite and hypersthene) and mono-mineralic amphiboles (hornblende, blue-green hornblende, tremolite-actinolite, and glaucophane) were separated from light-mineral fractions in beach, river, estuary, late-Pleistocene dune sheet deposits and latest-Holocene inner-

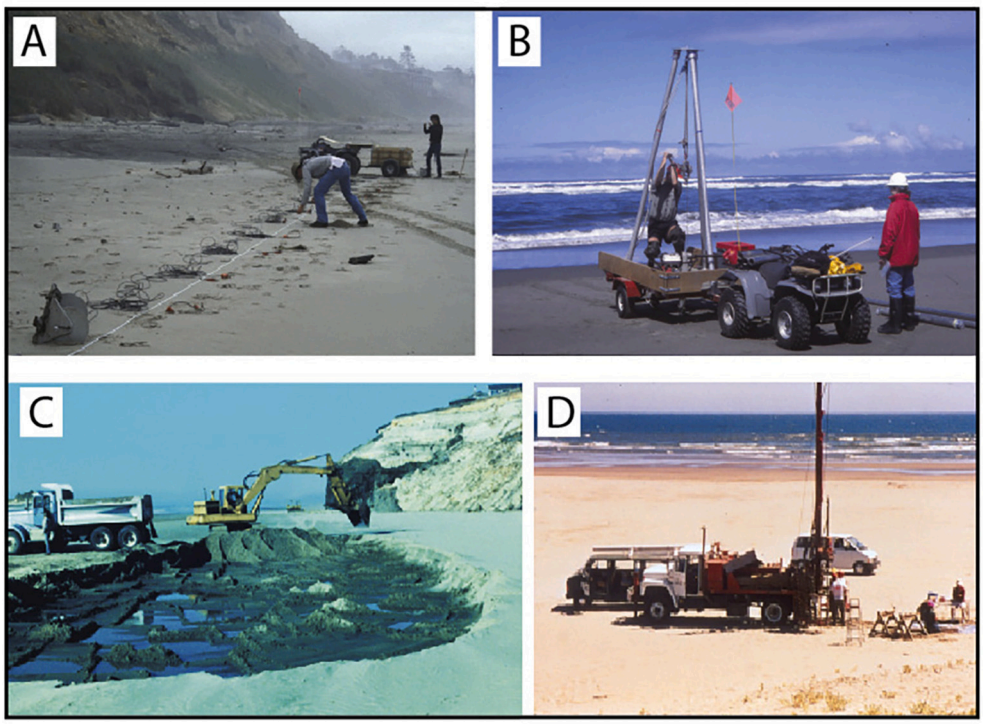

Fig. 6. Subsurface testing for beach sand thickness. A variety of methods were used to establish beach sand deposit thicknesses above wave-cut platforms 'bedrock' or basal cobble layers, including seismic refraction (Part A), vibracoring (Part B), mechanical backhoe (Part C), and solid-stem auger drill rig (Part D). The beach sand thickness above an indurated wave-cut platform in Part C (Newport subcell) is 1.0–1.5 m. The beach and innermost shelf sand thickness in Part D (Clatsop subcell of the CRLC) reached ~23 m below the prograded beach plain surface. Sand volumes of most active-beaches that are reported in this study are taken either to the wave-cut platform or to a maximum depth corresponding to about 5 m below the MLLW elevation (Pettit, 1990; Peterson et al., 1994). Deeper subsurface testing >10 m below subsurface was performed in the barrier and beach-plain backed beaches in the CRLC system (Herb, 2000; Vanderburgh et al., 2010).

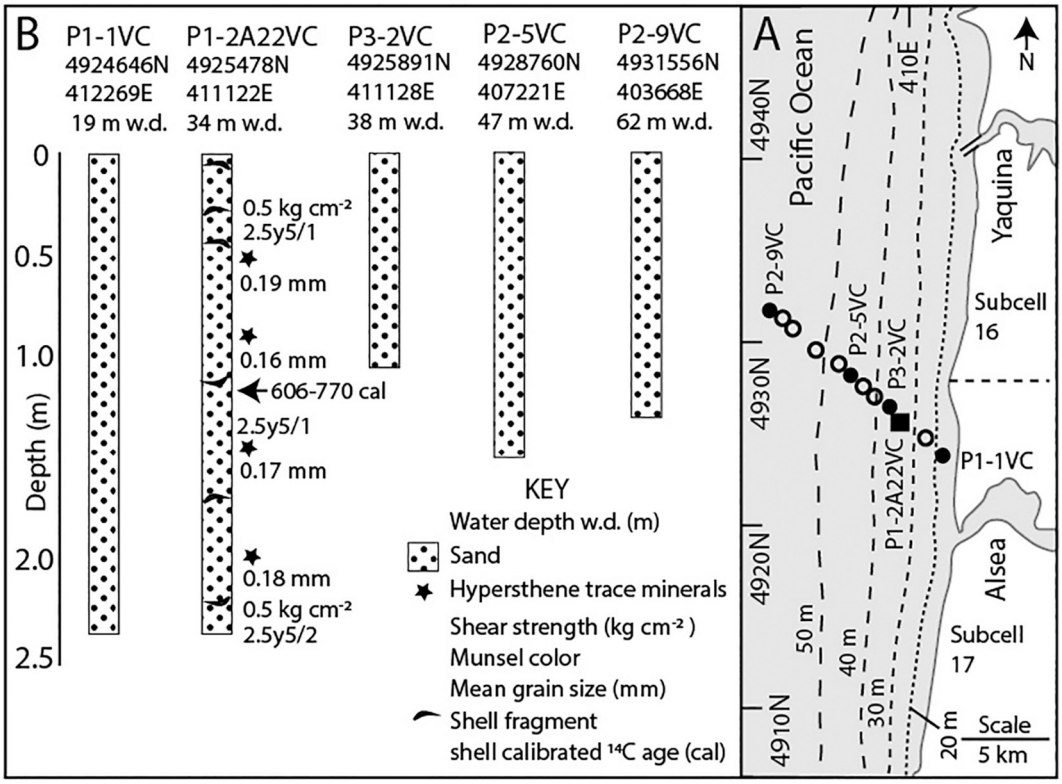

Fig. 7. Selected vibracores from the PacWave study area in the central Oregon inner-shelf. Vibracore sites (circles) are shown from the inner-shelf (19–62 m water depth) in the PacWave study area (Part A). Vibracores penetrated 0.9 to 2.3 m core subsurface depth in unconsolidated sand, without encountering transgressive ravinement surfaces of 1) basal cobble beds, 2) weathered dune soils, or 3) consolidated marine-terrace deposits (PacWave, 2019) Selected vibracore sites (solid circles) are keyed to vibracore logs, as shown in Part B. One vibracore P1-2A22VC (solid square), from 34 m water depth and of 2.31 m core length, was analyzed for 1) unconfined shear strength (kg cm^{-2}), 2) colour (Munsel), 3) mean sand grain size (mm), 4) trace-mineral hypersthene abundance, and 5) calibrated ^{14}C age of marine shell fragment (cal). The location of the PacWave study area is shown in Fig. 1. Heavy-mineral data are from Peterson and Kingen (2021).

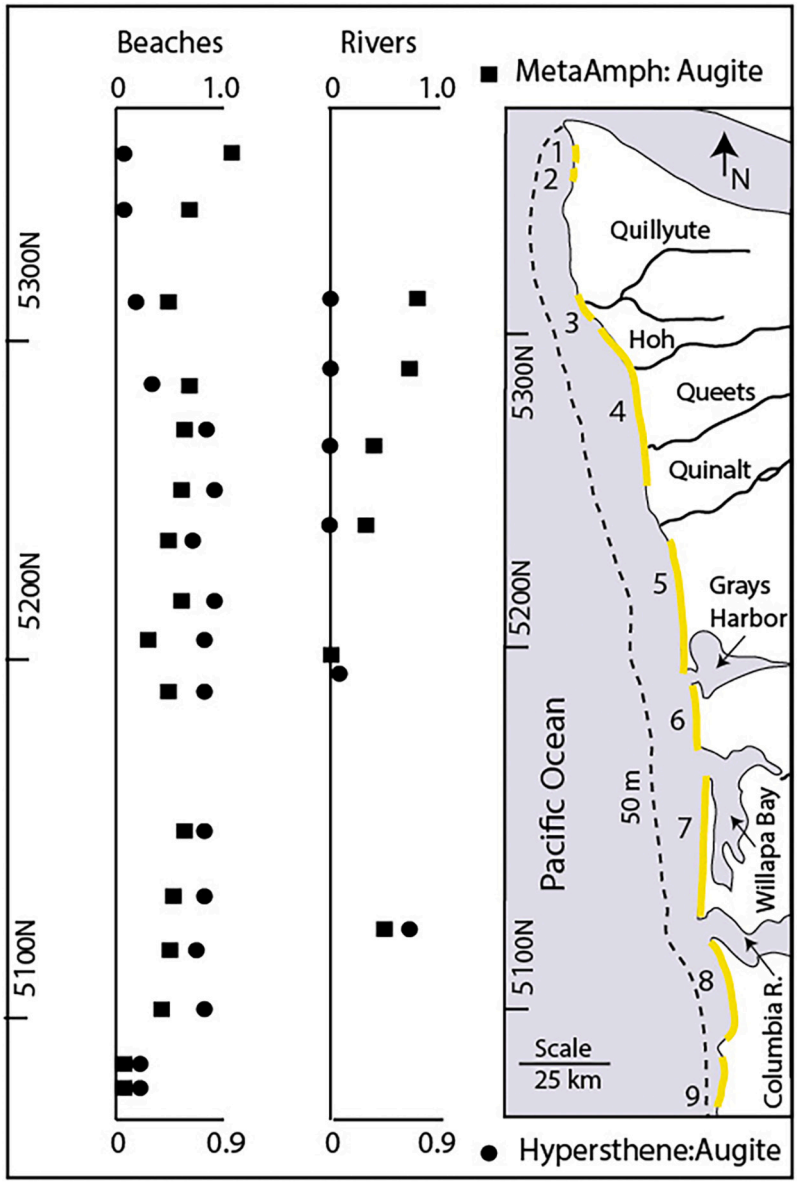

Fig. 8. Heavy mineral tracers for littoral sand sources in the northern PNW area. Map showing littoral subcells (yellow) surveyed for beach sand volumes (numbered 1–9) in the northern PNW study area (Table 1). Rivers (black lines) are named (Table 2), as are very large estuaries (arrows) in the CRLC system. The inner-shelf bathymetric contour (dashed line) is shown for the 50 m depth contour. Sand samples used for heavy-mineral analyses were collected from rivers and representative beach sites. Plots are shown for diagnostic heavy-mineral ratios including 1) hypersthene:augite (solid circles) and 2) metamorphic amphiboles:augite (solid squares). The metamorphic amphiboles (MetaAmph) analyzed here include blue-green hornblende, and actinolite-tremolite. Heavy-mineral data are from Peterson and Kingen (2021). (For interpretation of the references to colour in this figure legend, the reader is referred to the web version of this article.)

shelf deposits by centrifuge in Na-polytungstate (3.0 spg). The heavy minerals were mounted in picolyte™ for analysis under petrographic microscopy at 250× (300 grain counts per slide). Augite is largely derived from basalts in the uplifted North Coast Range drainages (Figs. 1 and 2) and flood basalts from eastern tributaries of the Columbia River (Glenn, 1960; Scheidegger et al., 1971; Venkatarathnam and McManus, 1973). Metamorphic amphiboles (blue-green hornblende, tremolite and actinolite) are largely derived from accreted terrains in the South Coast Range drainages and the Olympic Coast Range. Hypersthene is delivered from across the Coast Ranges via large antecedent rivers that reach intermediate volcanic rocks in Cascade volcanic arc. Glaucophane is derived from uplifted mélange rocks in the central California Coast Ranges, as represented by the Eel River, at the southernmost end of the PNW region.

A total of 26 subcells were surveyed for existing beach sand volume above the mean higher high water (MHHW) level and above the mean lower low water (MLLW) level. The MHHW beach surface level generally corresponds to the summer berm elevation. The MLLW beach surface level generally corresponds to the beach toe, or about 1.5 m below mean tidal level, or about 0.5 m below the 0 m NAVD88 elevation datum. The across-shore surveys or beach profiles were taken from either the foot of the sea cliff or the unvegetated seaward slope of a foredune to the beach toe or MLLW level during summer conditions (Peterson et al., 1994), and are referred to in this article as the active-beach part of the shoreline. In the PNW region, the active-beach areas are generally under public ownership and are open to public access, if they are not seasonally closed for protected species management.

The 26 surveyed subcell beaches total 657 km in alongshore length, or about 90% of the combined beach shorelines in the 34 subcells, as identified in Table 1. Those subcells that were not included in the beach sand volume surveys were deemed too inaccessible for reasons of 1) safety in handling seismic refraction charges, 2) exposure to strong runnel and rip currents during extended profile (beach toe/runnel) surveying, and 3) potential disturbance of protected species, including snowy plovers, sea lions, and northern elephant seals. Beach profile site locations were based on approximately even spacing and representative beach widths within each subcell (Pettit, 1990), as established by low elevation aerial- and video-reconnaissance imaging (Rosenfeld et al., 1991). Three profiles were collected, averaged, and/or compared for each profile locality to reduce bias from local beach width variability. The averaged locality profiles were then compared to the aerial photography/videography (at 0.5 km spacing) to adjust the computed

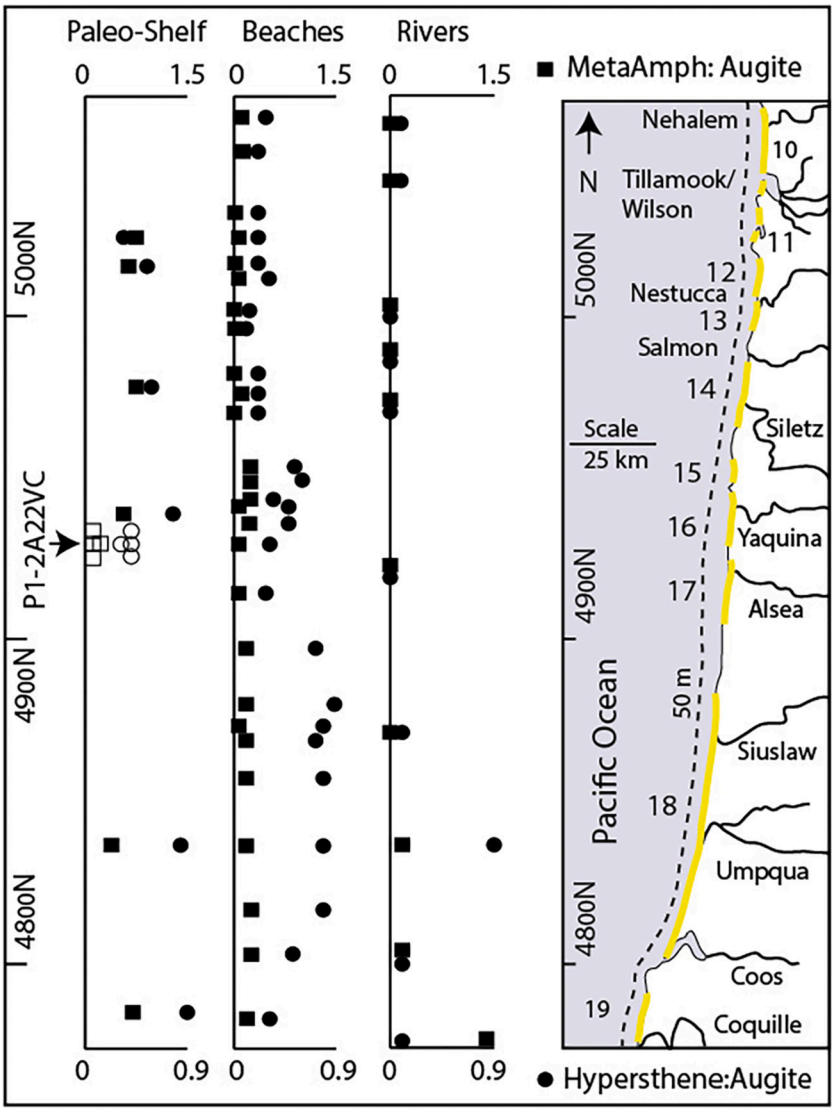

Fig. 9. Heavy mineral tracers for littoral sand sources in the central PNW area. Map showing littoral subcells (yellow) surveyed for beach sand volumes (numbered 10–19) in the central PNW study area (Table 1). Rivers (black lines) are named (Table 2), as are large estuaries (Tillamook bay and Coos Bay). The inner-shelf bathymetric contour (dashed line) is shown for the 50 m depth contour. Sand samples used for heavy-mineral analyses were collected from rivers, beaches, and sea cliff exposures of late-Pleistocene dune sheets that are thought to represent adjacent paleo-shelf deposits (Peterson et al., 2007). Plots are shown for diagnostic heavy-mineral ratios including 1) hypersthene:augite (solid circles) and 2) metamorphic amphiboles:augite (solid squares). The metamorphic amphiboles (MetaAmph) analyzed here include blue-green hornblende, and actinolite-tremolite. Paleo-shelf samples (solid shapes) are from late-Pleistocene dune sheets. Modern shelf samples (open shapes) are from the PacWave vibracore P1-2A22VC in 34 m water depth (Fig. 7). Heavy-mineral data are from Peterson and Kingen (2021). (For interpretation of the references to colour in this figure legend, the reader is referred to the web version of this article.)

beach cross-sectional areas by adjusted beach widths between survey mid-points (Pettit, 1990; Peterson et al., 1994). In addition to reducing potential bias from larger-scale beach width variability, the beach adjustment factors or beach width difference between the locality (reference) profile and the averaged (0.5 km spacing) profiles, also reflect beach volume measurement uncertainty. Computed beach adjustment factors (mean 1.02 ± 0.21 1σ, n = 127) in the study area (Peterson et al., 1994), suggest potential measurement uncertainties of ±20% in the beach sand volume estimates for individual profile segments. Collectively, the summed profile segments in the larger subcells (profile n = 5–18 per subcell) are assumed to reduce potential uncertainties to below ±20% beach sand volume.

The beach across-shore profiles (n = 153) were surveyed and tested for subsurface depths to wave-cut platforms (bedrock) or basal cobble layers. Subsurface tests of unconsolidated sand thickness were taken to depths of about −10 m subsurface or about 5 m below the MLLW tidal elevation datum. Beach profiling was conducted between 1990 and 1998 (Pettit, 1990; Peterson et al., 1994; Doyle, 1996; Meyers et al., 1996; Woxell, 1998; Percy et al., 1998; Herb, 2000; Vanderburgh et al., 2003; Vanderburgh et al., 2010). Subsurface profile imaging was performed by seismic refraction (beach backshore to mid-beach face) and ground penetrating radar (back-beach). Ground-truthing was performed by hand dug trenches, hand auger, vibracore, mechanical backhoe, and solid-stem auger drill rig (Fig. 6). Profile elevations were established by mid-swash runup during predicted mean tide level (±0.25 m vertical uncertainty). Soft-sand back-beach area sand volumes are established from back-beach surface area elevations (±0.1 m vertical uncertainty) using lidar in 2009 (DOGAMI, 2020) and in 2016 (U.S. Geological Survey, 2020) to measure average deposit thickness above the 0 m NAVD88 datum (Fig. 5) (Peterson et al., 2020b).

Inner-shelf profile gradients are measured at representative alongshore intervals within each subcell to establish sufficient profile gradients (≥ 0.40%) to ensure littoral sand dispersal and deposition across the innermost-shelf (Peterson et al., 2020a). In the central part of the PNW region, the interannual depth of closure is estimated to be ~20 m, as based on Army Corps of Engineers (USACE) dredge disposal sites in Region 10 that were monitored for disposal mound remobilizations (USACE, 1991a, 1991b; USACE, 2005b; USACE, 2006; USACE, 2012). Vibracores from the central subcells of the CRLC system demonstrate littoral sand vertical accretions of at least 1.0 m ka^{-3} to 40 m water depths, as ^{14}C dated over time scales of several centuries (Peterson et al., 2020a). For the purposes of this study, a conservative water depth of 30 m is assumed to represent the depth of closure, or the depth to which across-shelf littoral (beach-sourced) sand accumulation keeps pace with SLR, over the one century time scale. The 30 m water depth is used in this article to bound the seaward edge of the offshore (innermost-shelf)

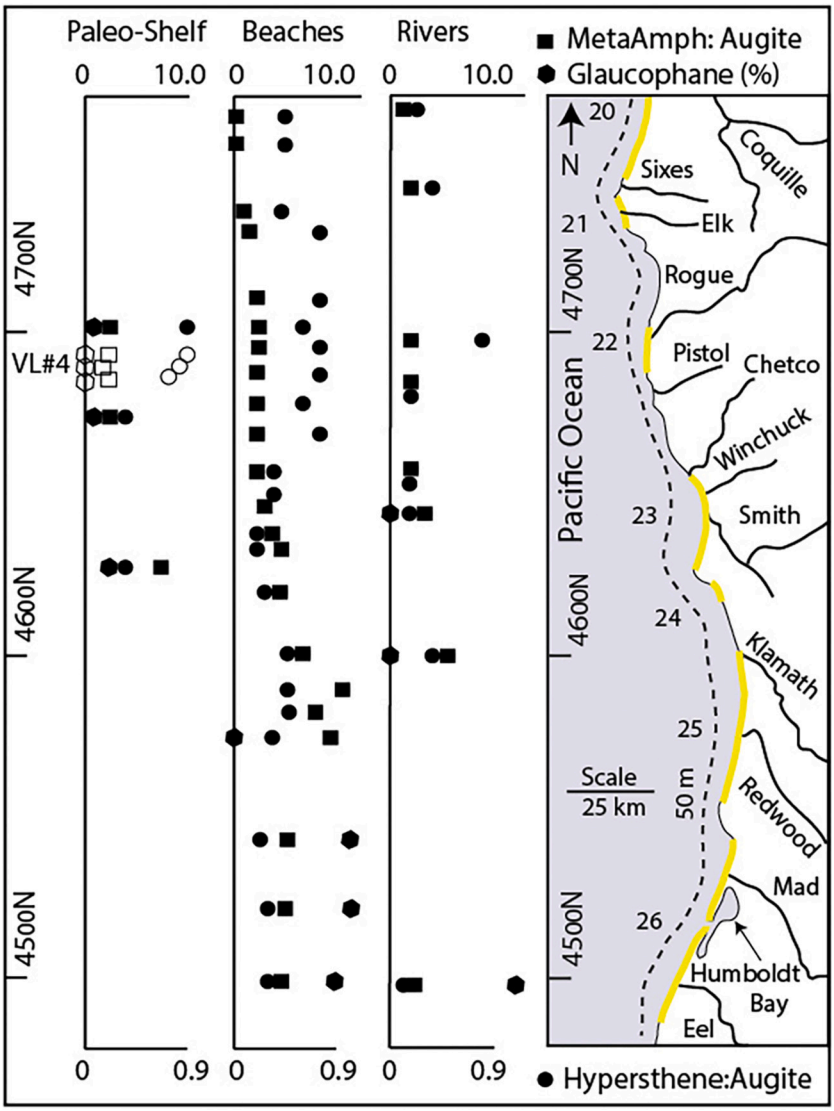

Fig. 10. Heavy mineral tracers for littoral sand sources in the southern PNW area. Map showing littoral subcells (yellow) surveyed for beach sand volumes (numbered 20–26) in the southern PNW study area (Table 1). Rivers (black lines) are named (Table 2), as is one large estuary (Humboldt Bay). The inner-shelf bathymetric contour (dashed line) is shown for the 50 m depth contour. Plots are shown for diagnostic heavy-mineral ratios including 1) hypersthene:augite (solid circles) and 2) metamorphic amphiboles:augite (solid squares). The metamorphic amphiboles (MetaAmph) analyzed here include blue-green hornblende, and actinolite-tremolite. Another metamorphic amphibole, glaucophane (solid polygon), is shown as percent (%) of total heavy-mineral count. Paleo-shelf samples (solid shapes) are from late-Pleistocene dune sheets. Modern shelf samples (open shapes) are from the Gold Beach vibralift station V4 (26 m water depth) (Fig. 3). Heavy-mineral data are from Peterson and Kingen (2021). (For interpretation of the references to colour in this figure legend, the reader is referred to the web version of this article.)

accommodation space, corresponding to the study region subcells. A transition zone of no net littoral (beach-sourced) sand accumulation (Bruun, 1962) is presumed for the inner 1/3 (0.33%) of the across-shore distance to the depth of closure. The inner and outer bounds of innermost-shelf accommodation space were contoured from across-shelf profiles as plotted from Google Earth Pro™ DEMs (Google Earth, 2020). The north and south terminations of the accommodation spaces are taken to be located at the subcell dividing headlands (Table 1; Fig. 4). The plotted innermost-shelf accommodation space areas were digitized with the Google Earth Pro™ polygon area calculator. Repeated digitization measurements resulted in maximum differences (uncertainty) of <1.0%.

Seasonally, reversing alongshore transport in the nearshore and innermost-shelf of the central PNW region is assumed to evenly distribute beach sand supplies within those subcell areas. However, net-alongshore transport likely plays an increasingly important role at the northern and southern areas of the PNW region, where some beach sand could be lost to 1) adjacent un-surveyed subcell areas, 2) the Juan de Fuca Strait, or 3) a submarine canyon, located offshore of the Eel River mouth, north of Cape Mendocino (Fig. 2) (Bodin, 1982). The greatest unaccounted losses of littoral sand from the innermost-shelf could occur from across-shelf sand transport to water depths greater than those of the innermost shelf. Though not evaluated in this study, the unaccounted potential uncertainty in offshore sand sinks all lead to underestimation of predicted offshore sand displacement. Therefore, the computed beach sand volume loss estimates reported in this article are considered to be conservative with regards to potential beach sand volume loss. In this article, predicted future beach erosion is largely estimated from increases in offshore accommodation space following sea level rise, which is the basis of Bruun's geometric equilibrium profile translation method (Bruun, 1962) and of the predictive modeling of future beach erosion in southern California (Erikson et al., 2017). In this article simplified block volume estimates of offshore accommodation spaces are used rather than cross-shore gradients (Erikson et al., 2017) due to bedrock platform control of some beach profiles and longshore transport within some subcells in the PNW region (Peterson et al., 2020b).

4. Results

4.1. Preliminary vibracore analyses from the inner-shelf of Central Oregon

A study area (PacWave), which is located offshore of subcells 16 and 17 in the central Oregon inner-shelf (Fig. 7), was vibracored to shallow subsurface depths (~0.5–2.5 m) as part of wave energy study locality in

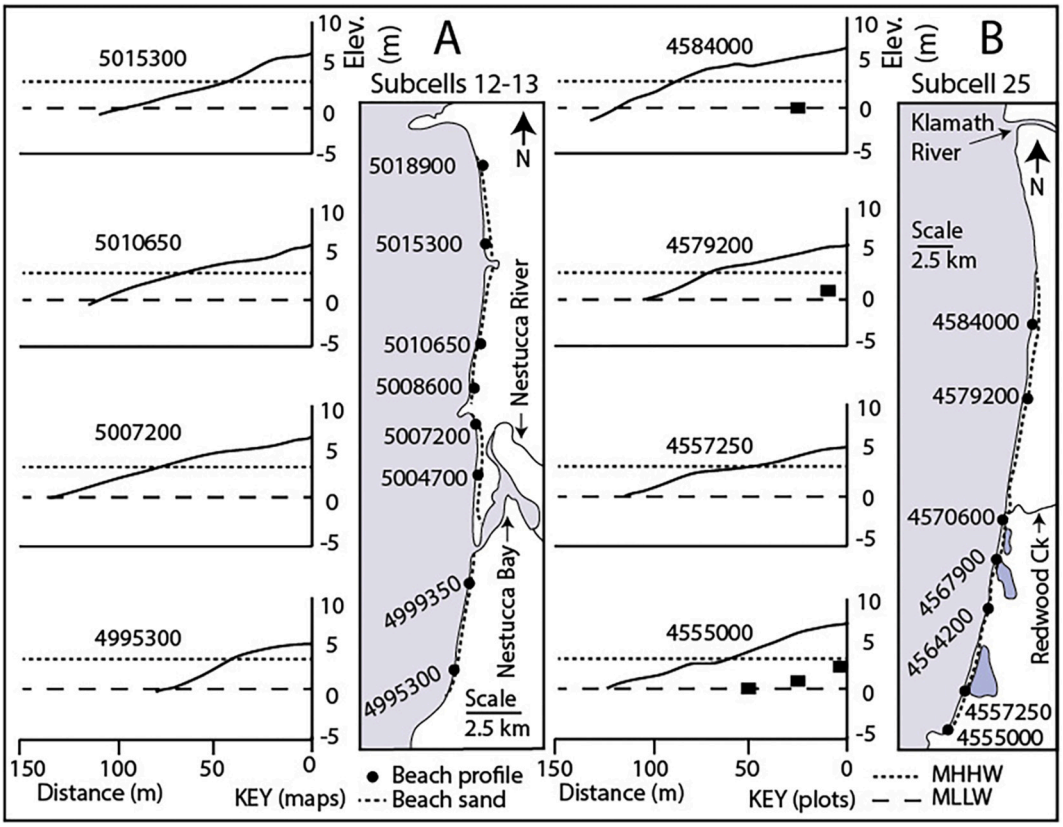

Fig. 11. Representative beach profiles in three PNW subcells (12, 13, and 25). Map of beach profile locations (solid circles with UTM-N coordinates) are shown for subcells 12 and 13 (Part A), and subcell 25 (Part B). Representative beach profiles (plots) are identified by profile location UTM coordinates and include summer beach sand surface elevations relative to MHHW and MLLW, and depth to the wave-cut platform, consolidated substratum or basal cobbles (solid squares). Summarized profile data are and subcell beach profile parameters are from Peterson and Kingen (2021).

2019 (PacWave, 2019). The PacWave study area is of particular importance to establishing depths to which seaward across-shelf sand transport occur, due to relatively uniform conditions of 1) modern beach width and grain size (Peterson et al., 1991), 2) offshore bathymetric contour orientations and along-shelf grain size distributions (Runge, 1966), and 3) modest values of coseismic-subsidence (~0.5–0.75 m) (Peterson et al., 2000). Additional simplifying conditions in the PacWave study area include a lack of very-large rivers, large ebb-tidal deltas, and/or major headlands, which could locally influence across-shelf transport). In this article, some preliminary results are shown from 12 representative vibracores from 19 to 62 m water depths, including one key vibracore (MSL1903)-P1-2A22VC from 34 m water depth. The 12 vibracores, as shown in Fig. 7, all terminated in unconsolidated medium fine sand. There are no traces of a buried transgressive ravinement surface, such as 1) basal cobble (beds), 2) late-Pleistocene dune soils (weathered), and/or 3) uplifted marine-terrace deposits (consolidated) in the 12 vibracores (PacWave, 2019). The vibracore P1-2A22VC deposits are characterized by low unconfined shear strength (~0.5 kg cm^{-2}), dark gray colour (2.5y5/2), and fine sand grain size (0.16–0.19 mm), which indicate a Holocene sand cover over the innermost-shelf study area. Elevated hypersthene:augite ratios (0.4–0.5) and low metamorphic amphibole:augite ratios (0.1–0.2) in vibracore P1-2A22VC sand samples confirm sand supply from the adjacent beaches and/or nearshore, but not the outer mid-shelf (Peterson et al., 2020b) (see detailed heavy-mineral analyses in Results Section 4.2 below). An AMS ^{14}C-dated bivalve shell fragment from 118 cm depth in vibracore P1-2A22VC (Beta 565,636) yielded the following age data: conventional 1510 ± 30 BP, adjusted 1120 ± 42 BP, and marine calibrated (MARINE13 and DeltaR 390 ± 29) 606–770 cal BP 2 σ (95.4%). A sedimentation interval of 750 years and 118 cm length yields a sedimentation rate of 1.6 m ka^{-1}, which is slightly greater than the estimated rate of latest-Holocene relative SLR (1.0 m ka^{-1}) in the study region (Peterson et al., 2019). Littoral sand supply to the inner-shelf has kept pace with SLR during very-latest Holocene time, at the cost of net beach sand loss in subcells 16 and 17, during the same time period (Hart and Peterson, 2007; Peterson et al., 2019). The apparent depth of closure (multi-century time scale) for littoral sand deposition in the inner-shelf of the central Oregon coast reached at least 34 m water depth.

4.2. Heavy mineral tracer analyses

Heavy-mineral analyses of modern beach and river sand samples in the northern part of the PNW region (Fig. 8) demonstrate the dominance of hypersthene-rich sand from the very-large antecedent Columbia River (Fig. 2) in modern beach sand deposits in subcells 5, 6, 7, and 8. Beach sand samples in the remaining subcells at the northernmost end of the PNW region show progressive increases in sand supply from local rivers draining the Olympic Coast Range (Peterson and Kingen, 2021). The Olympic Coast Range river sand supply is characterized by low hypersthene:augite ratios and high metamorphic amphibole:augite ratios, with increasing distance northward in subcells south-to-north 4, 3, 2, and 1. The local river sand supply could occur by direct entry into the littoral zone or by remobilized glacial outwash terrace deposits in eroding sea cliffs (Peterson et al., 2014a). Sand bypassing around minor headlands likely required some net-northward transport in the innermost-shelf. At the opposite (south) end of the northern PNW region, the modern beach sand in the southernmost subcell (number 9), is supplied by North Coast Range rivers that are dominated by augite, but not by Columbia River sand (Peterson et al., 2020b). Because no rivers directly enter subcell 9 the supply of augite-rich beach sand to that

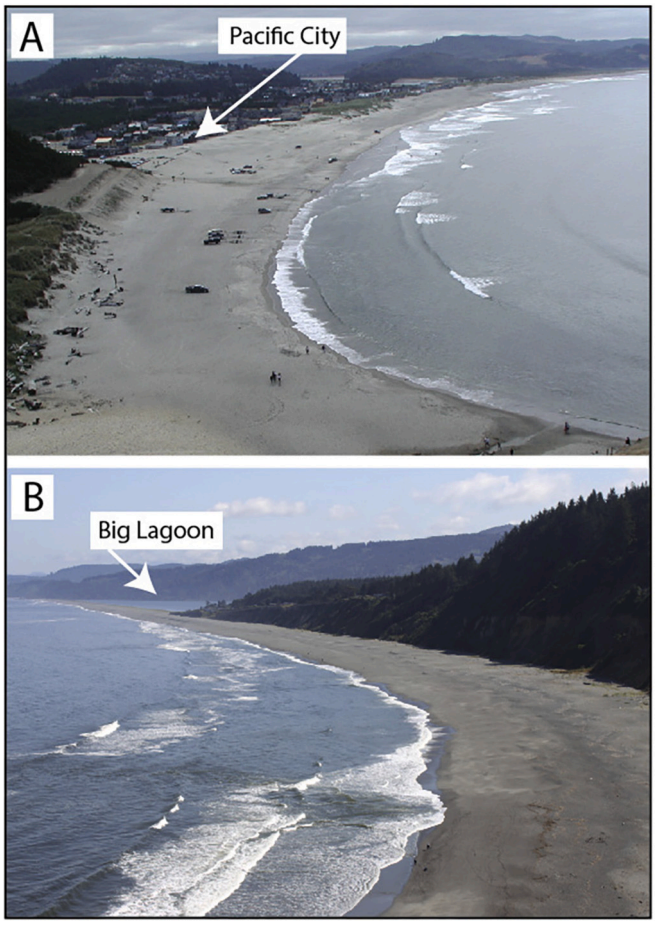

Fig. 12. Photos of two popular beaches susceptible to near-future SLR. Part A, Pacific City beach (profile 5007100) at the north end of subcell 12 (view is to the south). Pacific City (background) contains beach access improvements, private residences, commercial buildings, and public road/utility infrastructure (photo background) that could be threatened by soft-sand back-beach retreat, following potential near-future SLR. Part B, a Patrick's Point State Park beach at the south end of subcell 25 (view is to the north). This tourist destination beach (profile 4554720) could be lost from future SLR, leaving only basal cobble or wave-cut platform bedrock fronting the sea cliff. Such an offshore displacement of existing beach sand could also result in a breach of the narrow beach ridge that is protecting the freshwater lagoon (Big Lagoon in photo background), located immediately north of the sea cliff. See Fig. 11 for photo locations at identified beach profiles (UTM-N coordinates).

subcell is presumed to be derived from more southerly subcells, which are connected to the North Coast Range rivers, as presented below.

Littoral sand supplies to beaches in the central part of the PNW region (Fig. 9) include 1) local rivers, 2) paleo-shelf deposits, from transgressive sand supply and erosion of dune-sheet sea cliffs (Peterson et al., 2020b), and 3) longshore transport, with some bypassing around intervening headlands. For example, hypersthene-rich sand (hypersthene:augite ratio = 0.9) from the large antecedent Umpqua River (Fig. 2) dominates the beach sand mineralogy in subcell 18. Hypersthene-enriched beach sand components (hypersthene:augite ratios =0.5–0.9) diminish to the north in subcells 17, 16, and 15, and to the south in subcell 19. However, the supply of hypersthene to those beaches is complicated by the presence of significant hypersthene in late-Pleistocene dune sheet deposits (hypersthene:augite ratios =0.5–0.9), as exposed in eroding sea cliffs (Peterson and Kingen, 2021). Those dune sheets represent late-Pleistocene deposits that covered the middle and inner-shelf shelf (paleo-shelf) during marine low-stand emergence (Peterson et al., 2007). Remobilization and shoreward transport of some of those mid- and inner-shelf sand deposits, during the mid-Holocene marine transgression (9–5 ka), delivered sand to large Holocene dune sheets that are located landward of subcell 18. Some of the beach sand in subcells 15–19 could have been initially supplied by the mid-Holocene marine transgression (Peterson et al., 2020b). However, the central Oregon beaches and inner-shelf, including the PacWave vibracore site P1-2A22VC, are notably low in metamorphic amphiboles (metamorphic amphiboles:augite ratios =0.0–0.3), relative to the South Coast Range rivers (metamorphic amphiboles:augite ratios =1.6–5.4). The South Coast Rivers supplied the mid- and outer-shelf sand deposits by dominant northward littoral transport during late-Pleistocene shelf emergence (Scheidegger et al., 1971; Peterson et al., 2007). The dominance of hypersthene and augite in the modern beach and inner-shelf sand deposits in subcells 15–19 reflects substantial local river sand supplies from the Umpqua and North Coast Range rivers, well after the mid-Holocene marine transgression (Peterson et al., 2020b).

Beach sand mineralogies in the southern part of the PNW region (Fig. 10) reflect either 1) direct river sand supply from adjacent river mouths or 2) indirect river supply by alongshore transport from nearby river sources in adjacent subcells (Peterson and Kingen, 2021). For example, hypersthene-rich sand from the Rogue River (hypersthene:augite ratio = 0.8) influences beach sand mineralogies in subcell 22 and in adjacent beaches (hypersthene:augite ratios =0.6–0.8), and in late-Holocene inner-shelf deposits at vibralift Station V4 (hypersthene:augite ratios =0.7–0.9) (Fig. 3). A northeastward orientation of the coast, north of the Rogue River, likely explains the localized northward transport of Rogue River sand, in reverse to the general southward littoral transport in the southern PNW region (Peterson et al., 2009). Metamorphic amphibole-rich sands from the South Coast Range rivers dominate beach sand compositions (metamorphic amphibole:augite ratios =2.1–11.2) in subcells 23, 24, and 25 near the south end of the southern PNW region. Only subcell 26, located at the southernmost end of the southern PNW region, contains significant abundances of glaucophane (glaucophane =10–12%) as supplied by the Eel River (glaucophane =13%). Transport of Eel River glaucophane in modern beaches is restricted to subcell 26, demonstrating a limited northward littoral transport in subcell 26, due to its anomalous northeast shoreline orientation (Bodin, 1982; Peterson et al., 2009).

4.3. *Beach profiling and beach sand volume*

Beach profiles have been surveyed in 26 subcells in the PNW region (Fig. 2) to establish existing sand volumes in active-beach settings (Fig. 5). Several representative profiles are shown from the subcells 12 and 13 in the central PNW area, and from subcell 25 in the southern PNW area (Fig. 11). These subcells demonstrate some of the shoreline complexities in the PNW study region, and the associated variabilities in corresponding across-shore profiles. The Nestucca River/estuary delivered sand to subcell 13, but net-northward sand transport in the innermost-shelf delivered littoral sand around the minor bounding headland (between profiles 5007200 and 5008600) to feed sand to subcell 12, which lacks any other source of sand. In subcell 25, the large Klamath River delivered coarse sand and gravel via net-southward transport to broad beaches on either side of profile 4584000 and to narrower beaches, which extend southward to the beach-ridge barraged series of freshwater lagoons. The beaches shown in Fig. 11 are backed either by episodically eroded sea cliffs (hard back-beach areas) or unconsolidated sand deposits that extend below the 0 m NAVD88 datum in sandy back-beach deposits. The unconsolidated sand in back-beach areas typically include modern foredunes, estuary barrier spits, narrow beach ridges, and/or progradational beach plains. Whereas the potential loss of beach sand from sea cliff-backed shorelines results in intertidal beach cobble or wave-cut platform (bedrock), the potential loss of active-beach sand in soft-sand back-beach areas exposes the back-beach sand deposits to widespread erosion and shoreline retreat. For example, potential loss of the active-beach in the northern end of subcell 12 (Fig. 12A) would expose the public beach access areas, beach dory

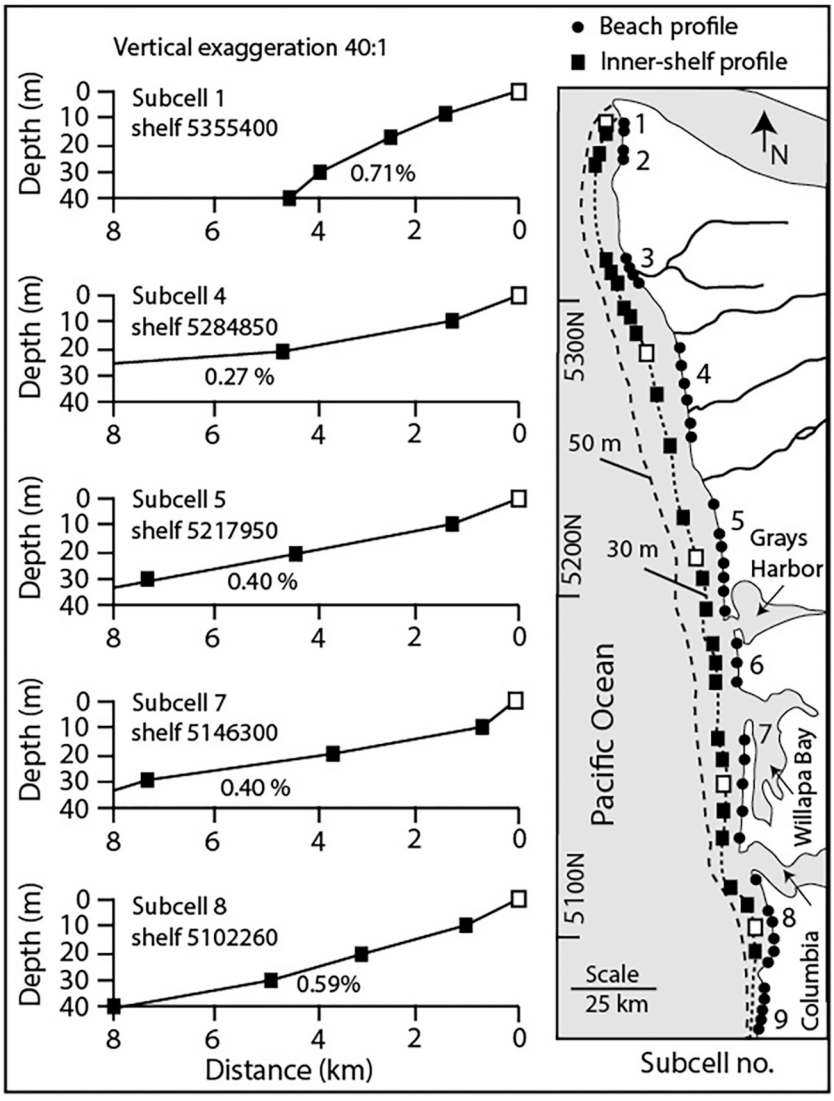

Fig. 13. Map of beach and inner-shelf profiles in the northern part of the PNW region. Beach profiles (circles) and inner-shelf profiles (squares) are shown in context with subcells (numbers) and inner-shelf bathymetry (30 and 50 m water depth contours). Open squares in the map correspond to representative inner-shelf profile plots. Representative inner-shelf profiles (identified by UTM-N coordinates) range from 0.27% to 0.71% in across-shelf gradient. See Tables 3 and 4, respectively, for beach and inner-shelf profile data.

launch, private residences, commercial buildings, and public road/utilities infrastructure in Pacific City, Oregon, to back-beach shoreline retreat. A loss of the active-beach in front of the sea cliff at the southern end of subcell 25 (Fig. 12B) would eliminate this destination beach in Patrick's Point State Park and threaten the narrow sand spit that protects the freshwater Big Lagoon, located just north of the sea cliff.

Beach profiles were collected at 153 locations in the 26 surveyed subcells (Figs. 13, 14, and 15). The profile UTM-northing positions, back-edge conditions, backshore elevations, beach platform depths, sand gain size distributions, beach widths and beach slopes (gradients) are shown for each profile in Peterson and Kingen (2021). The corresponding beach profile cross-sectional areas above the MHHW and MLLW tidal elevations, and corresponding alongshore beach segment lengths, and adjusted active-beach sand volumes above the MHHW and MLLW elevations are presented in Peterson and Kingen (2021). The setting and parameter data are summarized for each subcell below. Of the 153 beach profiles reported here, about 44% front episodically eroded sea cliffs (hard back-beach areas), and the remainder (56%) front foredunes, barrier spits, beach ridges, and/or prograded beach plains (soft-sand back-beach areas). The surveyed subcell shoreline distances total 657 km (Table 1), or about 65% of the PNW coastline (total length 1000 km). The remaining (un-surveyed) coastline is dominated by sea cliffs with very-narrow, discontinuous sand/gravel beaches (<50 m across-shore width). The shorelines backed by soft-sand back-beach areas represent ~40% of the total PNW coastline, or ~ 400 km in coastline length.

Across-shore profiles analyzed in the 26 surveyed subcells range from two to 18 in number (Figs. 13–15; Table 3) in approximate proportion to subcell length. Measured active-beach widths range from 62 m to 309 m in across-shore distance. Seventeen of the subcells contain significant extents of semi-contiguous soft-sand back-beach deposits (>10% of total subcell length). The soft-sand back-beach areas are analyzed for back-beach deposit erosion (average retreat distance) in Discussion Section 5.3. As expected, averages of mean sand gain sizes (0.12–0.60 mm) in the surveyed subcells increase with direct river sand supply to the subcell (Tables 1 and 2). Sand supplies from 1) river sand bypassing through large estuaries, such as the Columbia River estuary, 2) littoral sand bypassing around large headlands, and/or 3) paleo-shelf (dune sheet) deposits yield finer beach sand sizes, relative to direct river sand supply. Exceptions include subcell 22, which is connected to the Rogue River. However, mean grain size does increase south of the Rogue River mouth (profile grain sizes 0.33–0.43 mm), which is in the direction of dominant littoral transport in that subcell. Another exception is subcell 26 (grain size average 0.27 mm), which is supplied by the Eel River (Fig. 10). The Eel River tributary drainages are located in the central California Coast Range. Sediments from those drainages might differ in sand sizes or sand abrasion resistances in the surf zone, relative to the Cascadia margin rivers to the north. Computed beach sand

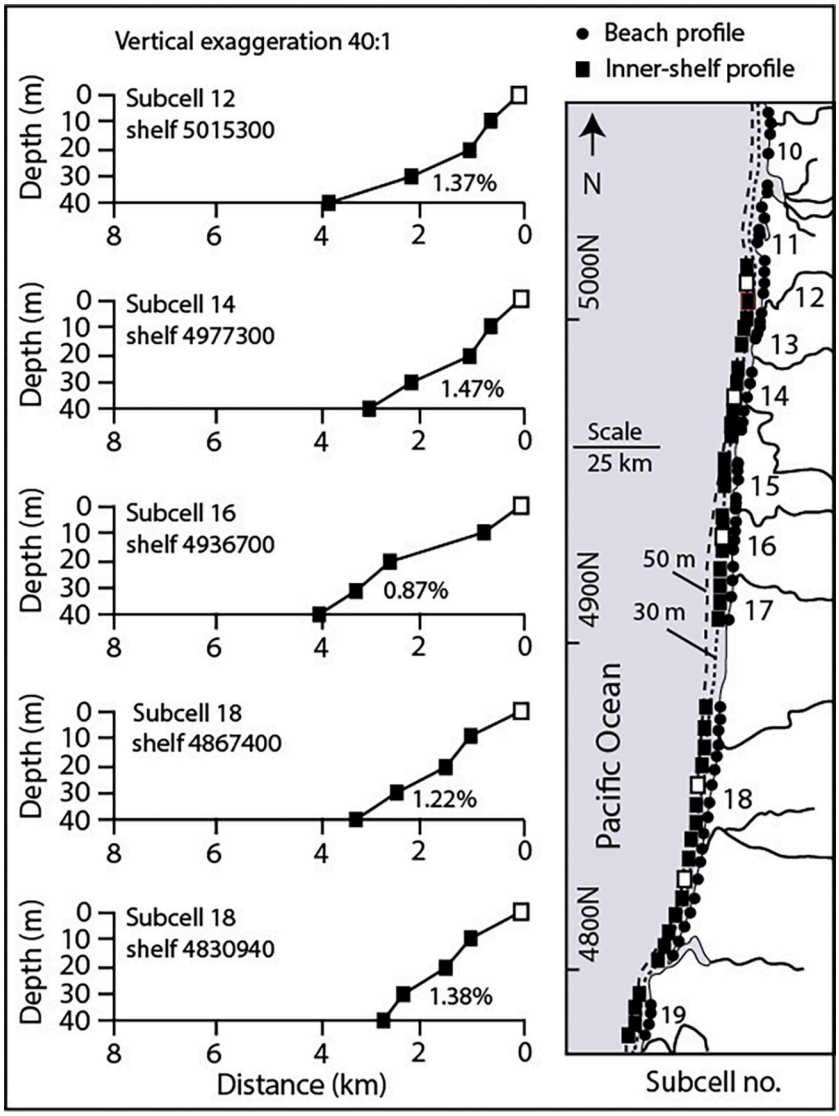

Fig. 14. Map of beach and inner-shelf profiles in the central part of the PNW region. Beach profiles (circles) and inner-shelf profiles (squares) are shown in context with subcells (numbers) and inner-shelf bathymetry (30 and 50 m water depth contours). Open squares in the map correspond to representative inner-shelf profile plots. Representative inner-shelf profiles (identified by UTM-N coordinates) range from 0.87% to 1.47% in across-shelf gradient. See Tables 3 and 4, respectively, for beach and inner-shelf profile data.

volumes for the 26 subcells range from MHHW ~0.2–22.1 × 10^6 m^3 to MLLW 0.4–48.1 × 10^6 m^3, as functions of summed profile sand cross-sectional areas and corresponding alongshore segment lengths. On average, the subcell beach sand volumes above MHHW are about 34% of the corresponding subcell volumes above MLLW in the 26 surveyed subcells.

4.4. *Inner-shelf gradients and depth-distance of innermost-shelf accommodation space filling*

The magnitudes of river sand supply and increasing submarine accommodation space volumes, including the inner-shelf and large estuaries, are the major drivers for beach sand displacements, following potential near-future SLR (Peterson et al., 2020a, 2020b). The key factors in controlling potential inner-shelf accommodation spaces are shelf gradients and corresponding shelf widths, to assumed littoral sand displacement depths of 30 m in the PNW region. Several hundred inner-shelf profiles were plotted to contour the seaward and landward bounds of the offshore accommodation spaces in the 26 surveyed subcells (Fig. 16). Key parameters from representative innermost-shelf profiles (n = 129), in approximate proportion and position to beach profiles (Figs. 13–15), are presented in Peterson and Kingen (2021). These parameters include 1) gradient and across-shelf distance to the 30 m water depth, 2) width of the transition zone (33% of the innermost-shelf width), and 3) width of the remaining offshore accommodation space. Several innermost-shelf areas are too shallow to accumulate littoral sand, as follows: subcell 4 between profiles 5284800–5254300 (gradients 0.0.27–0.30%), subcell 55,236,000 (gradient 0.35%), and subcell 23 between profiles 4635800–4626800 gradient (0.24–0.32%). The very-shallow innermost-shelf areas in subcells 4, 5, and 23 are identified as offshore rocky shoals in navigational charts. All the reported profile data (Peterson and Kingen, 2021) are averaged to characterize the innermost-shelf conditions for the 26 surveyed subcells (Table 4). Innermost-shelf accommodation space volumes of potential littoral sand accumulation are computed for 0.5 and 1.0 m vertical accretions of littoral sand, as presented in Table 4. The two different vertical accretions (0.5 and 1.0 m) are used to represent two different SLR values (0.5 and 1.0 m SLR) or two different sedimentation rates (0.5 m 100 yr^{-1} and 1.0 m 100 yr^{-1}) for the next century. Potential innermost-shelf accumulation volumes of littoral sand range between 2.6 × 10^6–105.7 × 10^6 m^3 and 6.2 × 10^6–211.5 × 10^6 m^3, respectively, for the 0.5 m and 1.0 m of beach sand vertical accretion in the innermost-shelf accommodation spaces.

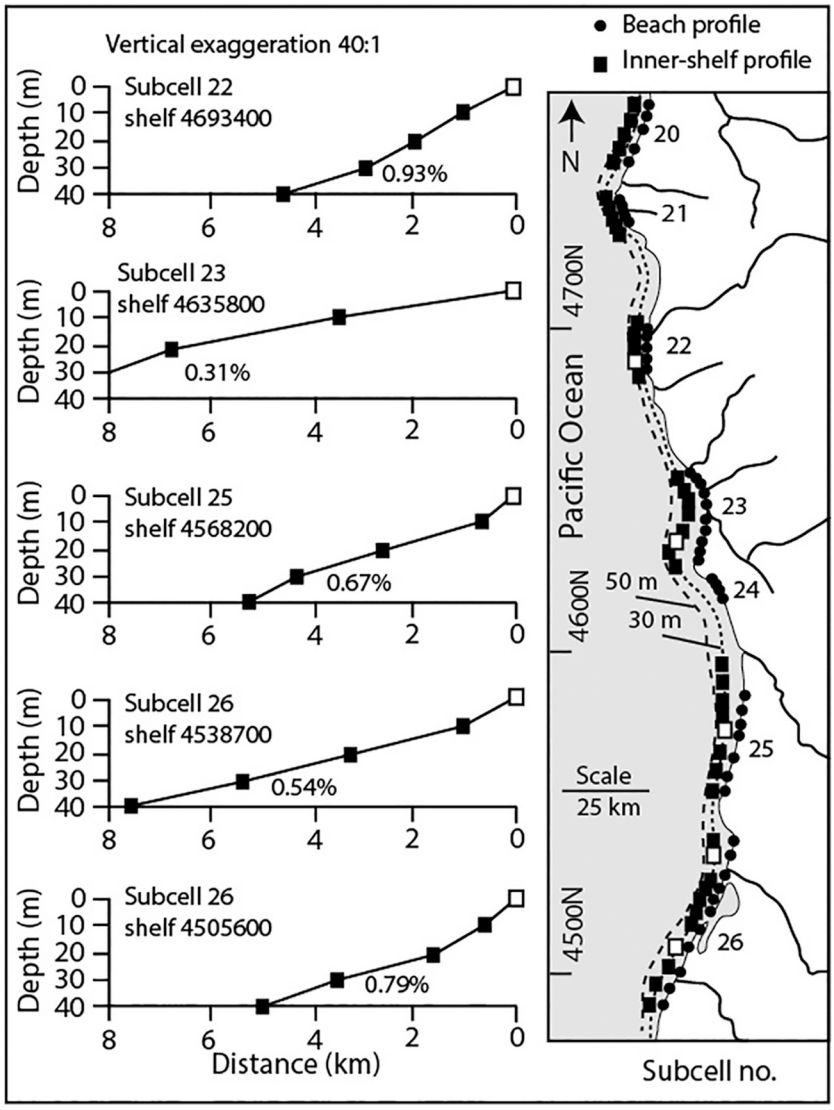

Fig. 15. Map of beach and inner-shelf profiles in the southern part of the PNW region. Beach profiles (circles) and inner-shelf profiles (squares) are shown in context with subcells (numbers) and inner-shelf bathymetry (30 and 50 m water depth contours). Open squares in map correspond to representative inner-shelf profile plots. Representative inner-shelf profiles (identified by UTM-N coordinates) range from 0.31% to 0.93% in across-shelf gradient. See Tables 3 and 4, respectively for beach and inner-shelf profile data.

5. Discussion

5.1. Estimated beach, river, estuary, sea cliff, and shelf littoral sand supplies and sinks

Existing beach sand volumes in 26 surveyed littoral subcells in the PNW region were previously presented in Table 3. River bedload sand supply to the PNW estuaries, or directly to the subcell beaches, were previously presented in Table 2. Those values are multiplied by 100 years to estimate river sand supply during the one century time period of potential near-future SLR, as shown in Table 5. Rivers without significant subtidal or intertidal surface areas are expected to deliver all of their annual bedload supplies to corresponding subcell beaches during the 100-year interval. Rivers entering estuaries with significant tidal surface areas require an additional step to establish possible river sand throughput to the adjacent subcell beaches. The proportion of river sand that is trapped in the estuary due to increasing accommodation space from SLR is based on the distribution, or percent surface area, of the river sand component in the estuary surface (modern) deposits below the mean tidal level (MTL), as previously shown in Table 2. Mud dominates the upper-intertidal levels in PNW estuaries (Peterson et al., 2020b), so accommodation spaces above the current MTL in the PNW estuaries are not evaluated in this article. Due to abundant sediment supply and high-energy sediment dispersal processes, the PNW estuaries have maintained sedimentation rates (1.0 m ka^{-1}) at the pace of SLR (1.0 m ka^{-1}) during latest-Holocene time (Glenn, 1978; Peterson and Scheidegger, 1984; Peterson et al., 2014b; Peterson and Vanderburgh, 2018a, 2018b). Those relations are used to predict both river and beach sand accumulations in the PNW estuaries following either a 0.5 or a 1.0 m sea level rise (Peterson et al., 2020b). The relative balances between the predicted river sand accumulations in the estuaries and the corresponding river bedload supplies, over the same time interval (100 years), represent the net surplus (adjusted volume) of river sand that could be throughput to the subcell beaches. River sand supplies during the next 100 years that fall short of river sand accumulations in corresponding estuaries, following either 0.5 or 1.0 m of SLR, are reported as $\times 10^6$ m^3 adjusted river sand supplies, as shown in Table 5. The accumulations of beach sand in the estuaries, following near-future SLR are also estimated using modern surface sediment compositions and surface areas below the mean tidal level (see Table 2), and net vertical accretions of either 0.5 m or 1.0 m, as presented in Table 5. Innermost-shelf beach sand sink volumes for the 0.5 m and 1.0 m SLR, or vertical accretion values are taken from Table 4. Summing of the existing beach volumes, adjusted river sand supply volumes, estuary beach sand sink volumes, and innermost-shelf beach sand sink volumes, for the 0.5 and 1.0 m SLR scenarios, within the next 100 years, is used to estimate the

Table 3
Summarized data for subcell beach profiles and totaled subcell beach sand volumes.

Subcell	Beach profiles (n)	Soft back -beach (%)	Ave. beach width (m)	Ave. beach slope (%)	Average grain size (mm)	MHHW sand volume ($\times 10^6$ m^3)	MLLW sand volume ($\times 10^6$ m^3)
1	2	80	192	1.7	0.17	1.2	3.8
2	2	0	141	3.1	0.26	0.5	2.2
3	4	20	99	5.0	0.45	0.2	0.4
4	6	0	81	4.3	0.51	1.5	19.3
5	7	55	309	1.5	0.19	7.7	35.7
6	3	100	251	1.9	0.22	5.7	18.3
7	5	100	249	2.2	0.25	9.7	35.8
8	6	85	253	2.7	0.22	13.9	30.5
9	5	10	158	2.7	0.17	1.4	3.7
10	6	100	97	4.3	0.21	5.7	15.5
11	6	60	62	4.9	0.20	0.2	2.8
12	4	60	65	5.6	0.24	0.8	2.8
13	4	100	93	4.9	0.31	1.4	5.5
14	7	20	134	4.2	0.43	2.9	5.0
15	4	0	126	3.1	0.23	0.1	0.7
16	7	20	134	1.9	0.18	1.4	4.6
17	4	25	117	2.3	0.18	2.4	9.4
18	18	100	155	3.8	0.33	22.1	48.1
19	4	35	139	3.3	0.28	3.0	7.1
20	6	75	135	5.6	0.39	2.8	7.4
21	5	15	113	5.2	0.46	1.8	3.6
22	6	17	160	3.8	0.28	2.9	4.4
23	10	70	104	5.5	0.58	3.5	9.0
24	4	10	118	2.0	0.12	0.2	6.3
25	7	60	78	5.5	0.60	2.9	9.7
26	11	95	167	4.0	0.27	9.7	22.0

Notes: Subcell data are averaged from subcell beach profile settings and subcell beach profile parameters in Peterson and Kingen (2021). Soft back-beach area extents (%) of subcell total beach lengths are refined with Google Earth (2020) satellite imagery and path measuring tools. Beach widths (m) are taken from the active-beach back-edges to mid-beach faces at mean tidal level (MTL) (Peterson et al., 1994). The beach slopes or gradients (%) are taken from the active-beach back-edges to the beach toes or mean lower low water (MLLW) levels. Beach sand volumes ($\times 10^6$ m^3) are calculated from adjusted profile cross-sectional areas (Pettit, 1990; Peterson et al., 1994) above the mean higher high water (MHHW) level and above the mean lower low water (MLLW) level. Those cross-sectional areas are multiplied by corresponding beach segment lengths, then summed to yield total beach sand volumes for each subcell. The EDM total station profiles are resolved to 1.0%. Uncertainties in alongshore variabilities in beach widths, measured tidal levels, and depth to bedrock in sea cliff-backed beaches lead to estimated uncertainty of ±20% beach sand volume in the larger subcells. The smallest beach sand volume is ~0.1 million cubic meters, so computed beach sand volumes are rounded to 0.1 million cubic meters.

resulting beach sand surplus (+) or deficit (−) for each of the 26 surveyed subcells (Table 5). The potential for new sand supply from retreats of semi-indurated late-Pleistocene beach and dune sand deposits in low sea cliffs of the central Oregon coast (Fig. 2) are presented in Table 6, as discussed below. New sand supply from unconsolidated (soft) sand deposits in active sand ramps of back-beach areas (Peterson et al., 2019), as well as, bay spits and dune deflation plains, are presented in Table 8, as discussed below in Section 5.3.

As previously noted in Background Section 2.1 large bedrock sea cliffs in northern Washington and Southern Oregon have not supplied sufficient sand to adjacent beaches (< 50 m width) to keep up with longshore transport and/or latest-Holocene SLR. However, semi-indurated dune and uplifted beach deposits in low sea cliffs of the central Oregon coast (Fig. 2) do share some mineralogic similarities to sand deposits in moderately wide beaches of the central Oregon coast (Fig. 9). The sea cliffs could have been significant sources of beach sand over millennial time scales in late-Holocene time (Peterson et al., 2020b). To estimate the relative importance of sea cliff sand supply in the near future (100 years) we project an average retreat distance of 50 m in 100 years for subcells 14, 15, 16, 17, 19, and 20 in the central Oregon coast (Table 6). This average is based on reported historic retreat rates of 0.25 m yr^{-1} (Priest, 1999) for the first 33-year period, a doubling of the retreat rate to 0.5 yr^{-1} m for the second 33-year period, and a tripling of the retreat rate to 0.75 m yr^{-1} for the third 33-year period. The average 0.5 m yr^{-1} retreat rate is multiplied by 100 years to yield an average 50 m retreat distance. That average value is multiplied by the semi-indurated dune/beach sand section lengths (km) and corresponding sand deposit thicknesses (m) to yield the potential retreat sand production volumes ($\times 10^6$ m^3). The reported modern sea cliff retreat rate and projected future rates are possibly over-valued. Rates of 0.25 m yr^{-1} and 0.5 m yr^{-1}, respectively, yield potential retreat distances of 250 and 500 m during the last 1000 years of 1.0 m SLR. Such great retreat distances would have precluded the preservation of beach platform stumps (1–3 ka in age) that are located less than 100 m in seaward distance from the modern sea cliffs (Hart and Peterson, 2007) (see Background Section 2.1). Nevertheless, the projected average sea cliff retreat (50 m in 100 years) and corresponding potential sand production volumes are compared to submarine accommodation space deficits (Table 5). The analyzed subcells yield potential sand production volumes that range from 5 to 11% of the corresponding subcell sand deficits (Table 6). Under the assumed 50 m of net shoreline retreat for the semi-indurated sea cliffs the estimated retreat sand production will not significantly diminish potential beach sand loss from the 1.0 m SLR for the next 100-year period. Furthermore, ongoing and likely accelerated construction of sea cliff revetments, including large rip-rap and/or concrete seawalls, could substantially reduce sea cliff retreat distances and associated sand production volumes to adjacent beaches in the central Oregon coast (Peterson et al., 2020b).

5.2. Regional comparisons of active-beach sand loss

Of the 26 PNW subcells evaluated for potential sand loss from near-future SLR, some 20 subcells are predicted to lose all of their active-beaches, on a subcell-averaged basis, from 0.5 m of SLR or vertical accretion in submarine accommodation spaces (Table 5). The active-beach areas, as defined in this article, extend seaward from back-edge sea cliffs or seaward foredune slopes to the beach toe (Fig. 5). Those 20 subcells that are predicted to lose all of their active-beach areas from a 0.5 m SLR represent 60% of the combined shoreline length of the 26 surveyed subcells (Table 1; Fig. 17). Surveyed subcells that will lose all of their

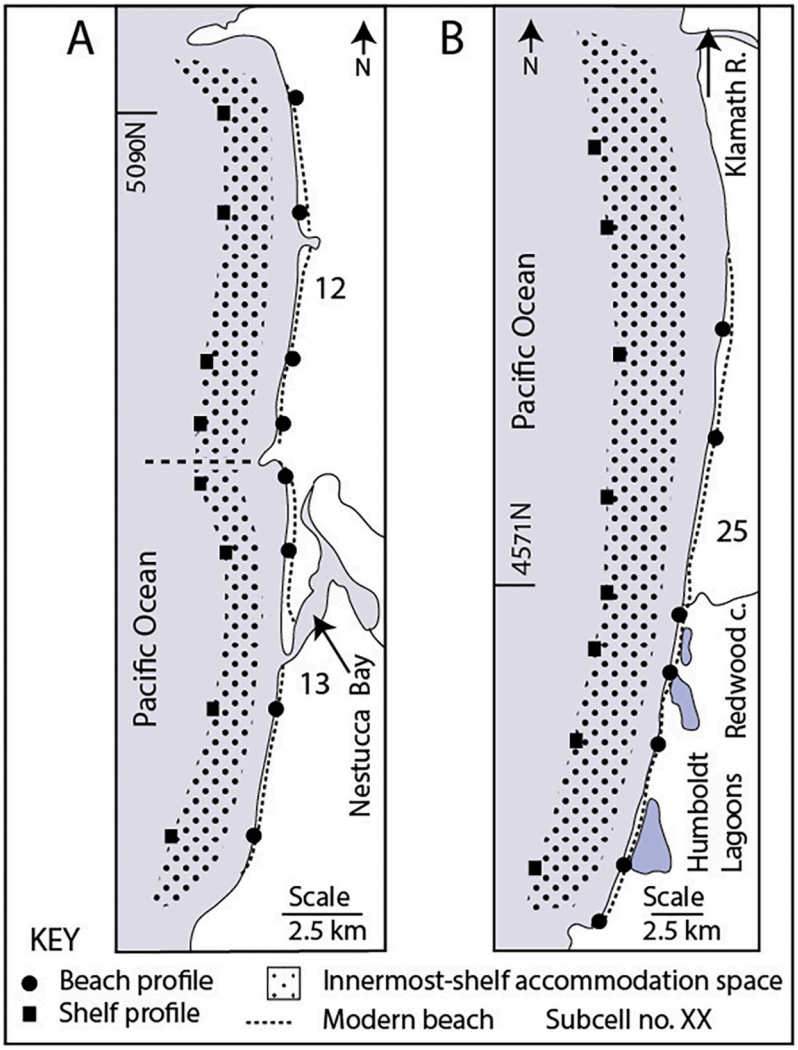

Fig. 16. Maps of innermost-shelf accommodation space areas in three subcells. Maps of offshore accommodation space areas (stippled) in the innermost-shelf ($\leq$ 30 m water depth), the transition zone (33% of the innermost-shelf width) and bounding headlands for subcells 12 and 13 (Part A), and subcell 25 (Part B). Positions of selected inner-shelf profiles (solid squares) and beach profiles (solid circles) are shown. The Nestucca River (Part A) likely feeds both subcells 13 and 12, as divided by a small headland (dashed line). The large Klamath River (Part B) delivers sand and gravel south to feed beaches and narrow beach berms (dotted lines) that front either prograded beach plains/sea cliffs north of Redwood Creek, or freshwater lagoons (Humboldt Lagoons) south of Redwood Creek.

active-beaches, on a subcell-averaged basis, from a 1.0 m of SLR or an equivalent of vertical littoral sand accretion in submarine accommodation spaces, total 23 in number. Those 23 subcells that will lose all of their active-beach areas from 1.0 m SLR represent 80% of the combined length of the 26 subcell beaches. The PNW beaches that are not included in the 26 surveyed subcells are, on average, narrower and shorter than those that are included in the 26 subcells and they (un-surveyed) account for about 25% of the total combined beach shoreline length in the PNW region (Peterson et al., 1994). Therefore, the loss of active-beaches for the entire PNW region, following 1.0 m of SLR, is estimated to be 90%, based on total alongshore beach length (~900 km) in the study region.

Beyond the catastrophic losses of active-beaches in the 23 subcells (Table 5), those subcells are also analyzed for sand loss deficits or the volumes of sand that are owed to the submarine accommodation spaces after the displacements of both existing beach sand reserves and any adjusted river sand supply are taken into account. The sand loss deficits for the 1.0 m SLR, or 1.0 m of beach sand deposition in the submarine accommodation spaces, are predicted to yield deficits that range from -2.0×10^6 m^3 in subcell 24 (5.0 km in length) to -292.7×10^6 m^3 in subcell 7 (43.7 km in length), and average -42 $\times 10^6 \pm 62 \times 10^6$ m^3 1σ ($n = 23$ subcells). The very-large deficits in subcell 7 are associated with 1) zero adjusted river sand supply, 2) a low gradient (wide) innermost-shelf (Fig. 13), and 3) a large littoral sand sink in Willapa Bay (MTL surface area of 252 km^2) (Table 2). The computations of deficits are important for two reasons. The deficits can be used to estimate retreat distances in soft-sand back-beach areas (Fig. 5), as discussed below in Discussion Section 5.3. The deficits also represent the relative time scales for beach recovery following possible termination of near-future sea level rise. Even if SLR were to be terminated after the 1.0 m rise, it could take centuries for some subcells that lack river or back-beach (retreat) sand supplies to rebuild their beaches, assuming that sea level is not substantially lowered after the predicted near-future SLR. The subcell beach erosion deficits therefore serve as proxies for the magnitude and duration of the catastrophic beach erosion hazard in the PNW region on the basis of each subcell.

Only three subcells, out of the 26 surveyed subcells, are shown to have sufficiently-large adjusted river sand supplies to maintain their current active-beach extents following the estimated sand displacements from 1.0 m of SLR (Table 5; Fig. 17). All three subcells (numbers 22, 24, and 25) are fed by large rivers with no intervening estuaries to capture their ample river sand supplies, which range from 71.5 $\times 10^6$ m^3 to 415.8 $\times 10^6$ m^3 for the next 100 years. However, all three of those subcells might be more susceptible to future SLR than is suggested in Table 5. For example, subcell 22 is supplied by Rogue River sand, which largely contributes to the surplus beach sand (45.3 $\times 10^6$ m^3) for that subcell (Table 5). But two adjacent subcells (Pistol and Nesika) are also supplied with Rogue River sand (Table 1 and Fig. 10) by combinations of alongshore transport and headland bypassing. The small Pistol River sand supply in the Pistol subcell (Tables 1 and 2) is transported south of the three linked subcells (Peterson et al., 2009, 2019). The combined alongshore length of the Pistol and Nesika subcells (16.5 km) exceeds

Table 4
Innermost-shelf profile data and predicted volumes of littoral sand accretions in offshore accommodation spaces.

Subcell No.	0–30 m Distance (m)	0–30 m Gradient (%)	Transition (33%) distance (m)	Accommodation space width (m)	0.5 m vertical accumulation volume ($\times 10^6$ m^3)	1.0 m Vertical accumulation volume ($\times 10^6$ m^3)
1	3525	0.88	1163	2362	4.7	9.5
2	2820	1.07	931	1889	2.6	5.2
3	3473	0.98	1146	2327	5.4	10.9
4	7973	0.44	1852	3760	14.9	29.9
5	7600	0.40	2508	5092	41.9	83.3
6	6498	0.47	2144	4354	34.8	69.6
7	7330	0.41	2419	4911	105.7	211.5
8	6740	0.48	2224	4516	48.2	96.5
9	2560	1.18	845	1715	13.7	27.4
10	2564	1.198	846	1718	22.9	45.9
11	2610	1.16	862	1749	12.4	24.8
12	2310	1.31	762	1548	8.6	17.2
13	1908	1.62	630	1278	9.8	19.6
14	2080	1.45	686	1394	16.2	32.4
15	2785	1.10	919	1866	6.9	13.9
16	2866	1.07	946	1920	18.7	37.5
17	2228	1.35	735	1492	13.1	26.3
18	2551	1.20	842	1709	69.0	138.0
19	2775	1.09	916	1859	15.2	30.5
20	1958	1.56	646	1312	16.4	32.8
21	3664	0.91	1209	2455	8.4	16.9
22	4083	0.78	1347	2735	15.3	30.6
23	8249	0.39	2722	5527	24.3	48.6
24	4105	0.73	1355	2750	4.1	8.3
25	4809	0.64	1587	3222	74.1	148.3
26	4204	0.77	1387	2816	79.6	159.3

Notes: Across-shelf (shore-orthogonal) distance (m) is to the 30 m innermost-shelf depth, as averaged from Peterson and Kingen (2021). Gradient (%) is of the innermost-shelf (0–30 m depth) as interpreted from Google Earth (2020). Transition distance (m) is based on 33% of the innermost-shelf width. Accommodation space width (m) is from innermost-shelf width, minus the transition zone width. Littoral sand accumulation volume ($\times 10^6$ m^3) is for vertical filling (0.5 and 1.0 m thickness) of the digitized innermost-shelf accommodation space (Fig. 16) for each subcell. Repeated digitizations of selected accommodation space areas yield measurement uncertainties of <1.0%. The smallest innermost-shelf accumulation volume is ~2.6 million cubic meters, so computed accumulation volumes are rounded to 0.1 million cubic meters.

the length of intervening subcell 22 (13.5 km), thereby more than doubling the potential offshore sand sink volume, and thus throwing the combined Rogue River extended-littoral-system into net deficit. Subcell 25 is also shown to have a net surplus of beach sand (27.3×10^6 m^3) following a 1.0 m SLR (Table 5). However, a possible 1.5 m SLR would yield an additional 74 million cubic meters of littoral sand loss to the innermost-shelf, thereby easily surpassing the 27.3 million cubic meters of sand surplus in subcell 24. Based on the potential conditions of 1.5 m SLR, the popular State Park beach at the south end of subcell 24 (Fig. 12B) would cease to exist. The greatest estimated beach sand surplus in the study area occurs in subcell 26, located at the southern end of the PNW region (Fig. 2). The very-large supply of Eel River sand (415.8×10^6 m^3 for the 100-year period), along with the high-gradient (narrow) innermost-shelf, combine to yield an estimated beach sand surplus of 267.2×10^6 m^3, following a 1.0 m SLR (Table 5). However, that estimate does not account for littoral sand loss to 1) the Eel submarine canyon located north of Cape Mendocino (Bodin, 1982) and 2) beach sand loss to the deeper inner-shelf or mid-shelf areas, due to reported storm/flood-intensified across-shelf transport (Cacchione et al., 1999; Traykovski et al., 2000; Ogston et al., 2004). More work is needed to account for potential beach sand loss from subcell 26, via both the submarine canyon and the episodic across-shelf transport processes, to better evaluate its susceptibility to near-future SLR. More broadly, river bedload supply to sandy beaches in Northern California and Southernmost Oregon could dimmish from increasing droughts, thought to reflect ongoing climate change in California (Mann and Gleick, 2015).

5.3. Estimated soft-sand back-beach area retreat distances

Back-beach retreat distances are estimated for subcells with significant soft-sand back-beach settings (Table 7), including prograded bay spits, beach plains, low elevation dune deflation plains (Peterson et al., 1994), and higher-elevation active (non-perched) late-Holocene sand ramps (Peterson et al., 2019). The estimated back-beach retreat distances or erosional beach step backs are proportional to the subcell sand deficits from predicted SLR of 0.5 and 1.0 m (Table 5). Specifically, the potential back-beach retreat distances are established from 1) subcell beach sand deficits, 2) alongshore lengths and thicknesses of the corresponding soft-sand deposits, and 3) corresponding submarine erosion areas (Fig. 5) (Peterson et al., 2020a). Reiterative optimization methods were used to find retreat distances that yielded eroded soft-sand deposit volumes equal to the estimated beach sand deficit volumes. The back-beach retreat area volumes are based on averaged deposit elevations or thicknesses, above 0 m NAVD88, for back-beach retreat distances of 1) 0–100 m, including the modern foredune, as stabilized by non-native invasive dune grass, and 2) 100–300 m or 100–500 m, including landward beach plains, dune deflation plains, or active (non-perched) sand ramps (Table 7). The submarine erosion areas are computed from the summed active-beach and back-beach retreat distances, assuming 1.0% basal erosion gradients. With the exception of subcells 5, 6, 7, and 8 in the CRLC system (Figs. 1 and 2), the estimates of back-beach retreat distances are limited to 500 m. The 500 m distance limit corresponds to −5.0 m MLLW at the beach toe, which was the limit of projected subsurface testing by seismic refraction (10 depth subsurface) in the mid-beach profile sites (Pettit, 1990; Peterson et al., 1994). Deeper subsurface testing by solid stem auger rig in the CRLC system (Vanderburgh et al., 2010) permitted greater depths of assumed submarine area erosion, corresponding to back-beach retreat distances of nearly 600 m for 1.0 m SLR. The reiterative optimization methods yield the required back-beach retreat distances and corresponding submarine erosion volumes to match the predicted beach sand deficit volumes for each of the 16 subcells, as presented below.

Back-beach retreat distances of soft sand deposits generally range from 10 m to 300 m for the 0.5 m SLR conditions and from 50 m to 610 m for the 1.0 m SLR conditions (Table 8). The two drivers for back-beach retreat distances are 1) the magnitude of the predicted beach sand

Table 5
Estimates of beach sand surplus or deficit following 0.5 and 1.0 m SLR.

Sub-cell	Beach reserve $\times 10^6 m^3$	0.5 m slr adj. river $\times 10^6 m^3$	0.5 m slr shelf $\times 10^6 m^3$	0.5 m slr estuary $\times 10^6 m^3$	0.5 m slr beach +/− $\times 10^6 m^3$	1.0 m sl adj. River $\times 10^6 m^3$	1.0 m slr shelf $\times 10^6 m^3$	1.0 m slr estuary $\times 10^6 m^3$	1.0 m slr beach +/− $\times 10^6 m^3$
1	3.8	0	4.7	0	−0.9	0	9.5	0	−5.7
2	2.2	0	2.6	0	−0.4	0	5.2	0	−3.0
3	0.4	3.1	5.4	0	−1.9	3.1	10.9	0	−7.4
4	19.3	4.8	14.9	0	+9.2	4.8	29.9	0	−5.8
5	35.7	0	41.9	27.0	−33.2	0	83.3	55.0	−102.6
6	18.3	0	34.8	27.0	−43.5	0	69.6	55.0	−106.3
7	35.8	0	105.7	58.5	−128.4	0	211.5	117.0	−292.7
8	30.5	0	48.2	0	−17.7	0	96.5	0	−66.0
9	3.7	0	13.7	0	−9.9	0	27.4	0	−23.7
10	15.5	1.8	22.9	1.4	−8.5	0.3	45.9	2.8	−32.7
11	2.8	0	12.4	2.9	−12.4	0	24.8	5.7	−27.7
12	2.8	0	8.6	0.6	−6.4	0	17.2	1.2	−15.6
13	5.5	0	9.8	0.3	−4.6	0	19.6	0.5	−14.6
14	5.0	0	16.2	0.5	−11.7	0	32.4	0.9	−28.3
15	0.7	0	6.9	0	−6.2	0	13.9	0	−13.2
16	4.6	0	18.7	1.8	−15.9	0	37.5	3.7	−36.6
17	9.4	0.39	13.1	0.9	−4.21	0	26.3	1.8	−18.7
18	48.1	41.4	69	8.3	+12.2	31.9	138	16.5	−74.5
19	7.1	1.8	15.2	0	−6.3	1.8	30.5	0	−21.6
20	7.4	1.8	16.4	0	−7.2	1.8	32.8	0	−23.6
21	3.6	1.3	8.4	0	−3.5	1.3	16.9	0	−12.0
22	4.4	71.5	15.3	0	+60.6	71.5	30.6	0	+45.3
23	9.0	13.2	24.3	0	−2.1	13.2	48.6	0	−26.4
24	6.3	0	4.1	0	+2.2	0	8.3	0	−2.0
25	9.7	165.9	74.1	0	+101.5	165.9	148.3	0	+27.3
26	22.0	415.8	79.6	5.7	+352.5	415.8	159.3	11.3	267.2

Notes: Common river sand supplies are split evenly between paired subcells (12–13 and 19–20). Multiple river sand sources are combined for those subcells that are fed by multiple rivers, including subcells 4, 10, 14, 18, 23 and 26 (Table 2). The Sixes and Pistol Rivers (Table 2) deliver river sand to small subcells (Table 1) that were not surveyed for this study. In the very-large Columbia River estuary (Figs. 2 and 8) the Columbia River sand supply is expected to balance increasing accommodation space in the estuary following a modest SLR (~1 m) over the one century time scale (Peterson et al., 2020a). Beach sand sinks in the large marine-dominated estuaries, Grays Harbor and Willapa Bay, are apportioned as follows: 1) subcells 5 and 6 deliver littoral sand equally to Grays Harbor and 2) subcell 7 delivers sand to Willapa Bay. The Willapa Bay littoral sand sink is conservative, as the subtidal areas in Willapa Bay (~40%) were not evaluated for littoral sand accumulation following latest-Holocene SLR (Peterson and Vanderburgh, 2018a). Several subcells host multiple estuary sand sinks, including subcells 10, 14, and 18. The uncertainties for summed subcell beach sand volumes are estimated to be ±20% (see Methods Section 3). Potential measurement errors for river annual sediment discharge are not reported by Karlin (1980), but the converted bedload supply volumes (Table 2) are computed to 1×10^3 m^3 yr^{-1}, or 0.1 million cubic meters for 100 years. Digitization uncertainties for the innermost-shelf accommodation space areas are estimated to be <1.0%. Larger potential uncertainties could arise from littoral sand loss to inner-shelf water depths greater than 30 m, making the beach sand deficits greater than reported. The smallest beach sand deficit volume is less than 1.0 million cubic meters, so computed surplus or deficit volumes are rounded to 0.1 million cubic meters.

Table 6
Estimates of potential beach sand supply from eroding sea cliffs of semi-indurated dune and beach sand.

Subcell	Semi-indurated sand total length (km)	Semi-indurated sand average thickness (m)	Retreat distance (m)	Retreat sand volume ($\times 10^6$ m^6)	Sea cliff sand supply relative to deficit (%)
14	3.0	17.0	50	2.5	9
15	1.0	13.0	50	0.7	5
16	5.5	10.1	50	2.7	7
17	5.0	4.6	50	1.1	6
19	1.5	14.0	50	1.0	5
20	4.0	13.4	50	2.6	11

Notes: Sea cliff sections of semi-indurated sand (late-Pleistocene beach and dune sand) in six representative subcells (14, 15, 16, 17, 19 and 20) are totaled for length (km) and average thickness (m), as taken at 0.5 km intervals from representative measured sections (Peterson et al., 2006). Sea cliff sections with >10 m basal bedock exposed above the backshore sand level or > 15 m thickness above the 0 m datum (NAVD88) are excluded, as are all sections protected by engineered revetments (large rip-rap, concrete and/or shotcrete). Sections with less than 1.5 m of semi-indurated dune/beach sand thickness above bedrock at the sea cliff are excluded. Subcell positions are presented in Table 1. Estimated potential sea cliff sand productions average under the 10% level of significance for 5 of the 6 subcells and only 11% (marginally significant) for the most southernmost subcell (20).

deficit (Table 5) relative to soft-sand segment length and 2) the back-beach deposit thickness, as averaged over the width of the back-beach retreat areas. Some of the largest back-beach retreat distances are predicted to occur within the large CRLC system (Figs. 1 and 2), including 550 m in subcell 6, and 590 m in subcell 7 for 1.0 m of SLR. Adding active-beach retreat distances of 250 m for subcells 6 and 7, respectively, yield total retreat distances of 800 m (subcell 6) and 840 m (subcell 7). Previous estimates of shoreline retreat, as based on different methods of estimating back-beach retreat volume for 1.0 m SLR (Peterson et al., 2020b), are 700 m each in subcells 6 and 7. Large back-beach retreat distances (>500 m) for 1.0 m SLR are also estimated for short soft-sand back-beach areas in subcells 11, 14, and 16. Those central PNW region subcells are characterized by short segments of soft-sand deposits in short bay spits, relative to much longer sea cliff-back shorelines and associated offshore accommodation spaces. By comparison, only 50 m of averaged back-beach retreat for 1.0 m SLR is estimated for subcell 18, which is characterized by 1) a modest sand deficit volume relative to subcell length, 2) significant adjusted river sand supply, and 3) large foredunes. A back-beach retreat distance of 160 m for 1.0 m SLR in subcell 10, compares to a previous estimate of 180 m (Peterson et al., 2020b), which did not include submarine eroded volumes.

6. Conclusions

In this article, evidence is presented that leads to predictions of catastrophic losses of existing active-beach areas in the PNW region,

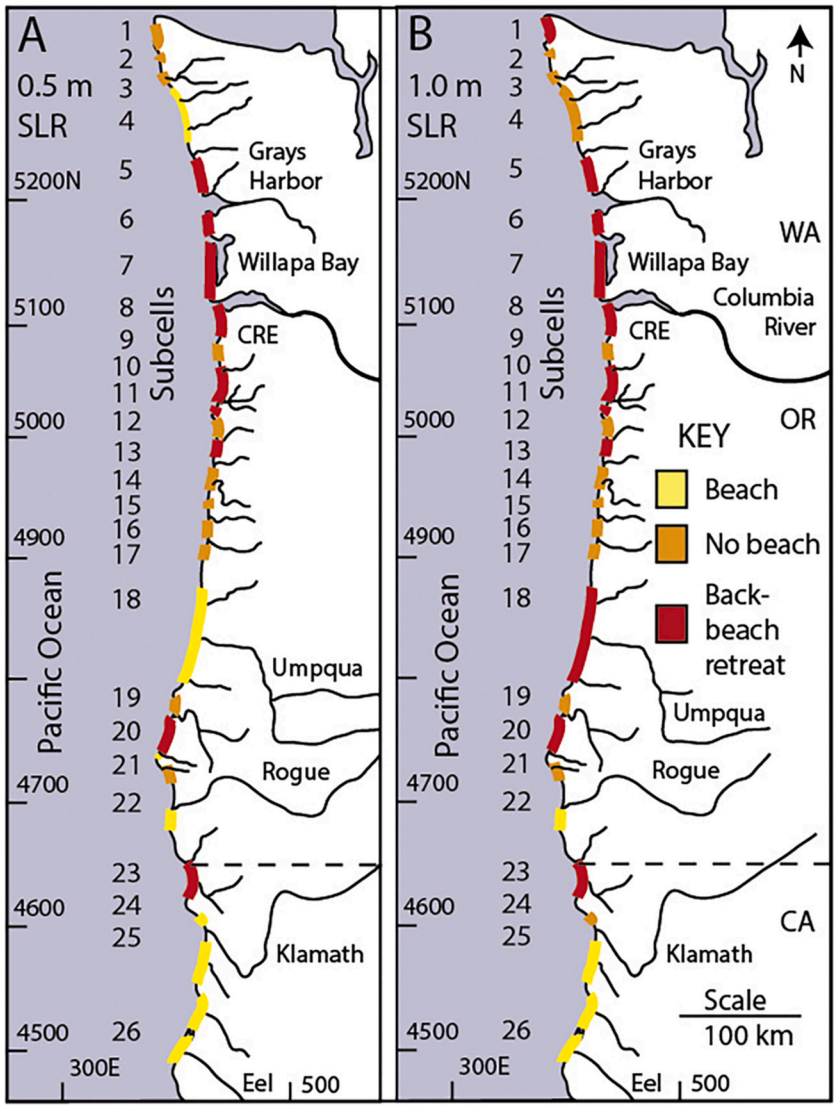

Fig. 17. Predicted beach conditions following potential 0.5 m and 1.0 m SLR in the PNW region. Maps show predicted beach conditions in 26 analyzed subcells (numbered) in the PNW region following potential near-future SLR of 0.5 m (Part A) and 1.0 m (Part B) or equivalent littoral sand vertical accretions (0.5 and 1.0 m thickness) in subcell submarine accommodation spaces. Predicted beach conditions include, 1) active-beach preservation (yellow), 2) active-beach erosion to sea cliffs or vegetated foredunes (orange), and 3) dominant back-beach retreat in unconsolidated sand spits, dune fields, or beach plains (red). Very large estuaries are named, including the Columbia River Estuary (CRE), Willapa Bay, and Grays Harbor. Large sediment-supply rivers are named, including the Columbia, Umpqua, Rogue, Klamath, and Eel Rivers (Table 2). (For interpretation of the references to colour in this figure legend, the reader is referred to the web version of this article.)

following potential near-future SLR. In the 26 subcells analyzed for beach sand displacements to future increase in submarine accommodation spaces, 60% and 80%, respectively, of the active-beaches, by alongshore lengths, are predicted to be lost from 0.5 and 1.0 m of SLR, within the next century. Projections of these relations to narrower unsurveyed subcell beaches in the study area indicate a 90% loss of all (combined) beach lengths within the PNW region, from a potential near-future SLR of 1.0 m. Sand supply from indurated bedrock sea cliffs have not kept pace with latest-Holocene rates of longshore transport and/or SLR (1.0 m ka^{-1}) in the study region, so are not assumed to supply significant sand to eroding beaches over the near-future scenario conditions of 1.0 m SLR in one century. Similarly, projected sea cliff erosion rates and associated new sand deposits from the retreats of semi-indurated late-Pleistocene dune and beach deposits are not predicted to significantly reduce beach volume sand loss from near-future SLR (1.0 m). Beyond the loss of current active-beach areas, the predicted increases in submarine accommodation space volumes for displaced littoral sand, including the innermost-shelf and large estuaries, will demand sand-supply well in excess of most measured beach sand volumes. The erosion deficits will impact soft (sandy) back-beach areas with net retreat distances in unprotected eolian sand ramps, bay spits, beach plains, and/or dune deflation plains. The erosional step back of soft shoreline beaches will likely be reduced or eliminated by shoreline hardening in many developed back-beach areas that are privately owned. Supratidal beaches will be replaced by intertidal -to- subtidal sand/gravel bars in front of the constructed revetments. Equally important, the large beach-sand deficits could delay any future beach recovery, in those subcells without river or back-beach retreat sand supplies for several centuries after the next century of SLR, if the future sea level is not lowered (sea level fall) following the predicted near-future SLR.

In this study site-specific retreat distances of semi-indurated sandy sea cliffs are not established due to 1) local variability of sea cliff material compositions, heights, and landward (subsurface) continuities, and 2) likely future stabilizations by revetments. Site-specific geotechnical studies will be needed to predict sea cliff basal-truncations, oversteepened slopes, slope failures, and net retreat distances of non-stabilized sea cliffs from near-future SLR. In any case, neither erosion nor artificial stabilization of the sea cliffs will not protect the adjacent sandy beaches from erosion. The supratidal sandy beaches will be replaced by intertidal bedrock platforms, variably covered by thin patches of gravel, algae or barnacle/mussel beds.

The controlling factors for beach sand surplus or deficit, following potential near-future SLR in the PNW region, are 1) river sand supply, 2) innermost-shelf littoral sand sinks, 3) large estuary sinks of beach and river sand, and 4) existing beach sand reserves. At the regional scale, the

Table 7
Settings of soft-sand back-beach segments in subcells with beach sand deficits from predicted SLR.

Sub-cell	Sandy back-beach segment UTM-N (m)	0.5 m SLR segment alongshore length (m)	0.5 m SLR segment active- beach width (m)	0–100 m back-beach thickness (m)	100–300 m back-beach thickness (m)	100–500 m back-beach thickness (m)	Back-beach setting
1	5355700–5351100	4600	190	14	9	8	Beach plains
5	5221400–5197700	23,700	300	11	4	7	Bay spit
6	5195100–5177300	17,800	250	10	4	8	Beach plains
7	5166800–5125000	41,800	250	8	7	8	Bay spit
8	5119100–5096400	22,700	250	22	20	14	Beach plains
10	5063240–5039300	23,900	100	7	7	7	Bay spit(s)
11	5028820–5023790	5030	60	9	5	6	Bay spit
12	5017000–5010300	6700	60	14	9	10	Bay spit
13	5007500–4994700	12,800	90	15	13	9	Bay spit
14	4975600–4971700	3900	170	13	10	6	Bay spit
16*	4940300–4938100	2200	180	9	8	7	Bay spit
17	4924000–491700	4300	100	13	12	11	Bay spit
18	4884008015	82,500	150	16	14	14	Dune plains
19	4781400–4775600	5800	100	14	9	12	Bat spit
20	4769300–4750500	18,800	120	13	11	12	Dune plains
23	4644000–4626900	17,100	100	9	5	8	Bay spit

Notes: Subcells with soft-sand back-beach areas (Peterson and Kingen, 2021) and net beach sand deficits (Table 5) for either 0.5 or 1.0 m sea level rise (SLR) are numbered. The alongshore extents of sandy beach shoreline segments are shown by UTM-northing coordinates (m) and shoreline length (m), as refined by Google Earth Pro™ images (Google Earth, 2020). Active-beach widths (m), as used to estimate submarine erosional areas, are averaged for the back-beach segments from Table 3 and Subcell beach profile parameters in Peterson and Kingen (2021). Averaged back-beach deposit thicknesses, above 0 m NAVD88 (Fig. 5) are computed from averaged deposit surface elevations for back-beach retreat distances of 0–100 m (including the modern foredune), and either 100–300 m or 100–500 m (including landward beach/dune plains). The back-beach elevation data are derived from Oregon State lidar 2009 (DOGAMI, 2020) and California and Washington States lidar 2016 (U.S. Geological Survey, 2020), both with reported vertical resolution of at least 0.1 m. The lidar elevation data are averaged with ArcGIS Pro™. Repeated digitization and ArcGIS Pro™ averaging of back-beach surface elevations for different retreat distances lead to thickness uncertainties ±15% of in the extensive low-relief spits, beach plains, and dune deflation plains, so deposit thickness is rounded to the nearest meter.

Table 8
Estimated retreat distances for soft-sand back-beach segments from 0.5 and 1.0 m SLR.

Sub-cell	0.5 m SLR submarine erosion thickness (m)	0.5 m SLR total eroded volume ($\times 10^6$ m^3)	0.5 m SLR back-beach retreat distance (m)	1.0 m SLR submarine erosion thickness (m)	1.0 m SLR total eroded volume ($\times 10^6$ m^3)	1.0 m SLR back-beach retreat distance (m)
1	0.07	0.9	10	0.41	5.7	80
5	0.57	33.1	110	2.13	102.6	430
6	1.39	43.5	280	2.74	106.3	550
7	1.52	128.3	300	2.95	292.5	590
8	0.17	17.5	30	0.62	66.1	120
10	0.23	8.5	50	0.82	32.7	160
11	1.51	12.4	300	>2.5	N/A	>500
12	0.33	6.4	70	0.89	15.6	180
13	0.11	4.6	20	0.36	14.6	70
14	1.13	11.7	230	>2.5	N/A	>500
16*	>2.5	N/A	>500	>2.5	N/A	>500
17	0.35	4.2	70	1.51	18.7	300
18	N/A	N/A	N/A	0.27	74.4	50
19	0.37	6.3	70	1.47	21.6	300
20	0.14	7.2	30	0.45	23.5	90
23	0.07	2.1	10	0.89	26.4	180

Notes: Average submarine erosion thicknesses (m) are taken from submarine erosion areas below the 0 m NAVD88 datum, based on landward and seaward basal erosion gradients (1.0%) and total retreat distance from the beach toe or beach face interception with MLLW (Fig. 5). The total eroded volumes ($\times 10^6$ m^3) include both the back-beach retreat area volumes and the submarine eroded volumes for the lengths of the subcell soft-sand back-beach segments, which nearly equal (within 0.2 $\times$ 10^6 m^3) the predicted subcell beach sand deficits for either 0.5 m or 1.0 m SLR (Table 5). Back-beach retreat distance estimates are limited to a maximum of 500 m, with an averaged submarine erosion depth of 2.5 m, for all subcells, other than those in the large CRLC system. The soft-sand shoreline segment in subcell 16* is very short, 2200 m in length (Table 6), yielding the anomalous >500 m retreat estimate for 0.5 m SLR. The estimated measurement uncertainties for back-beach retreat distances are driven by beach sand volumes (±20% uncertainty) and back-beach area digitization and elevation averaging (±15% uncertainty), totaling ±35% summed known uncertainties. Because beach sand deficits are potentially conservative or underestimated, due to the 30 m water depth cut-off for offshore sand displacements, the back-beach retreat distances could also be conservative. The estimated back-beach retreat errors do not account for recessed shorelines that are protected by deep embayment or by artificial stabilization with beach sand replenishment, stone rip-rap, and/or concrete seawalls. The smallest computed back-beach retreat distances are less than 100 m, so back-beach retreat distances are rounded to 10 m distance.

largest beach sand deficits are predicted to occur in the Columbia River Littoral Cell (CRLC) system. Although the CRLC beaches have the largest existing beach sand volumes, the wide innermost-shelf and large marine-dominated estuaries provide substantial sinks for beach sand, following potential SLR (0.5–1.0 m) during the next century. The very-large beach sand deficits in the central CRLC subcells are predicted to result in very-large total retreat distances (800–840 m) in barrier spits and beach plains, following a 1.0 m SLR. Modest net deficits of beach

sand are predicted to occur in the northernmost PNW region and throughout the central PNW region from 0.5–1.0 m SLR, due to 1) small river sand supplies, 2) modest innermost-shelf widths, and 3) small active-beach sand reserves. However, several small bay spits could experience >500 m of back-beach retreat, due their short lengths relative to their total subcell lengths and associated inner-shelf accommodation spaces. Several subcells in the southern part of the PNW region are predicted to maintain beach sand surpluses, following 0.5–1.0 m SLR, largely due to very-abundant river sand supplies. The application of the accommodation space methods, as used in this article to predict the responses of the PNW subcells to potential near-future SLR, should have broad application to studies of other threatened beaches in complex littoral systems worldwide.

An extended data file in PDF format (Peterson and Kingen, 2021) used for this paper is published in:

Peterson, C.D. and Kingen, K.E.P., 2021, Pacific Northwest Littoral Data. Dataset. https://doi.org/10.15760/geology-data.01.

Declaration of Competing Interest

The authors declare that they have no known competing financial interests or personal relationships that could have appeared to influence the work reported in this paper.

Acknowledgements

Ken Scheidegger assisted with petrographic microscopic analyses of reference heavy-mineral grains. Mark Darienzo assisted with aerial photo/video analyses of beach widths and coastal physiography in the PNW study area. Phil Jackson assisted with directing beach profiling in the PNW study area. Jon Kimerling and Doann Hamilton, respectively, designed and populated the database used in the beach profiling aspects of this study. Debra Doyle completed the beach profiling in the Tillamook, Sand Lake, and Pacific City subcells. David Percy and Ken Cruikshank completed the beach profiling in the Netarts subcell. Gary Carver and Lori Dengler provided logistical support for beach profiling in the Orick and Eureka subcells. Jim Phipps, mike Roberts, Loraine Woxell, and April Herb assisted with beach profiling and subsurface testing in the Columbia River Littoral Cell system. Maureen Walczak assisted with sample selection from PacWave (2019) vibracore MSL1903-P1-2A22VC. Kennett Peterson assisted with early manuscript editing. This research was funded by the National Coastal Resources and Development Institute, under the Coastal Zone Management Program, Oregon, grants No. 2-5632-03 and CZ17.90-5635-01, and the U.S. Geological Survey, Coastal and Marine Geology Program, under the South West Washington Coastal Erosion Project, Co-op #1434-HQ-96-AG-01612, and the NOAA Office of Sea Grant and Extramural Programs, U.S. Department of Commerce, under grant number NA76RG0476, project number R/SD-04, and by appropriations made by the Oregon State Legislature.

References

Arneson, R.J., 1975. Seasonal Variations in Tidal Dynamics, Water Quality, and Sediments in the Coos Bay Estuary. M.S. Thesis. Oregon State University, Corvallis, Oregon.

Atwater, B.F., Tutte, M.P., Schweig, E.S., Rubin, S.M., Yamaguchi, D.K., Hemphill-Haley, E., 2003. Earthquake recurrence inferred from paleoseismology. Dev. Quat. Sci. 1, 331–350.

Baker, C.A., 1978. A Study of Estuarine Sedimentation in South Slough, Coos Bay, Oregon. M.S. Thesis. Portland State University, Portland, Oregon.

Baker, D., Peterson, C., Hemphill-Haley, E., Twichel, D., 2010. Holocene sedimentation in the Columbia River Estuary. Mar. Geol. 273, 83–95.

Baldwin, E.M., Beaulieu, J.D., Ramp, L., Gray, J., Newton, V.C., Mason, R.S., 1973. Geology and Mineral Resources of Coos County, Oregon. Oregon Department of Geology and Mineral Industries, Bulletin 80, p. 82 with maps.

Bamber, J.L., Oppenheimer, M., Kopp, R.E., Aspinall, W.P., Cooke, R.M., 2019. Ice sheet contributions to future sea-level rise from structured expert judgment. Proc. Natl. Acad. Sci. 116, 11195–11200.

Barnett, E.T., 1997. Potential for Coastal Flooding Due to Coseismic Subsidence in the Central Cascadia Margin. M.S. Thesis. Portland State University, Portland, Oregon.

Barnhart, R.A., Boyd, M.J., Pequegnat, J.E., 1992. The Ecology of Humboldt Bay, California: An Estuarine Profile (Vol. 1). US Department of the Interior, Fish and Wildlife Service Biological Report, p. 121.

Barrick, R.C., 1976. Hydrodynamics of Grays Harbor estuary, Washington. Appendix A. In: Knott, N.P., Barrick, R.C. (Eds.), Maintenance Dredging and the Environment of Grays Harbor, Washington. U.S. Army Corps of Engineers, Seattle District, p. 16.

Bodin, P., 1982. Longshore and Seasonal Variations in Beach Sand Humboldt County, Calfornia: Implications for Bulk Longshore Transport Direction. M.S. Thesis. Humboldt State University, Arcata, California.

Briggs, G., Peterson, C., 1995. River versus beach mineral sources for estuary sand deposits and target paleotsunami deposits in Winchester Bay and the Lower Umpqua River Estuary. Unpublished Supplemental Report to U.S. Geological Survey. National Earthquake Hazard Reduction Program, Denver, Colorado.

Brunel, C., Sabatier, F., 2009. Potential influence of sea-level rise in controlling shoreline position on the French Mediterranean Coast. Geomorphology 107, 47–57.

Bruun, P., 1962. Sea-level rise as a cause of shore erosion. J. Waterw. Harb. Div. 88, 117–132.

Bruun, P., 1988. The Bruun rule of erosion by sea-level rise: a discussion on large-scale two-and three-dimensional usages. J. Coast. Res. 4, 627–648.

Cacchione, D.A., Wiberg, P.L., Lynch, J., Irish, J., Traykovski, P., 1999. Estimates of suspended-sediment flux and bedform activity on the inner portion of the Eel continental shelf. Mar. Geol. 154, 83–97.

Calib7.10, 2020. Radiocarbon Calibration Program. CALIB REV7.1.0. http://calib.org/calib/calib.html. Accessed June 05, 2020.

Clifton, H.E., Connard, G.G., Fisher, J., Fox, D., Mardock, C., McMurray, G., O'Brien, R. J., Peterson, C., Starr, R., Woolsey, R., 1990. Cruise report 1990 Oregon placer mineral research cruise (Al 90WO) September 21–October 3, 1990. In: U.S. Geological Survey, Open-File Report 91-279, p. 81.

Clifton, H.E., Peterson, C.D., Connard, G., 1991. Geology and geophysics. In: Preliminary Resource and Environmental Data: Oregon Placer Minerals, Joint State-Federal Oregon Placer Minerals Technical Task Force, Oregon Department of Geology and Mineral Industries, Open-File Report 0-91-02, pp. 9–74.

Cooper, J.A.G., Pilkey, O.H., 2004. Sea-level rise and shoreline retreat: time to abandon the Bruun Rule. Glob. Planet. Chang. 43, 157–171.

CREDDP, 1983. Columbia River Estuary Data Development Program. Bathymetric Atlas of the Columbia River. Astoria, Oregon, p. 16.

Cruikshank, K.M., Peterson, C.D., 2017. Late-stage interseismic strain interval, Cascadia subduction zone margin, USA and Canada. Open J. Earthq. Res. 6, 1–34. http://www.scirp.org/journal/ojer. https://doi.org/10.4236/ojer.2017.61001.

Darienzo, M.E., Peterson, C.D., 1990. Episodic tectonic subsidence of late-Holocene salt marsh sequences in Netarts Bay, Oregon, Central Cascadia Margin, USA. Tectonics 9, 1–22.

Davidson-Arnott, R.G., 2005. Conceptual model of the effects of sea level rise on sandy coasts. J. Coast. Res. 21, 1166–1172.

DeConto, R.M., Pollard, D., 2016. Contribution of Antarctica to past and future sea-level rise. Nature 531, 591–597.

DOGAMI, 2020. Lidar. Department of Geology and Mineral Resources. https://www.oregongeology.org/lidar/. Accessed July 15, 2020.

Doyle, D.L., 1996. Beach Response to Subsidence Following a Cascadia Subduction Zone Earthquake along the Washington-Oregon Coast. M.S. Thesis. Portland State University, Portland, Oregon.

Erikson, L.H., O'Neill, A., Barnard, P.L., Vitousek, S., Limber, P., 2017. Climate change-driven cliff and beach evolution at decadal to centennial time scales. Coast. Dyn. 2017, 125–136.

Glenn, J.L., 1960. Late Quaternary Sedimentation and Geologic History of the North Willamette Valley, Oregon. Ph.D Thesis. Oregon State University, Corvallis, Oregon.

Glenn, J.L., 1978. Sediment sources and Holocene sedimentation history in Tillamook Bay, Oregon. In: U.S. Geological Survey Open-file Report 78-680. Denver, Colorado, p. 64.

Google Earth, 2020. Google Earth Pro. https://www.google.com/earth/. Accessed June 20, 2020.

Hart, R., Peterson, C., 2007. Late-Holocene buried forests on the Oregon coast. Earth Surf. Process. Landf. 32, 210–229.

Herb, A.A., 2000. Holocene Stratigraphy and Sediment Volumes for the Columbia River Littoral Cell, Pacific Northwest, USA. M.S. Thesis. Portland State University, Portland, Oregon.

Horton, B.P., Khan, N.S., Cahill, N., Lee, J.S., Shaw, T.A., Garner, A.J., Kemp, A.C., Engelhart, S.E., Rahmstorf, S., 2020. Estimating global mean sea-level rise and its uncertainties by 2100 and 2300 from an expert survey. npj Clim. Atmos. Sci. 3, 1–8.

Jones, N., 2015. Modern surface sediment distribution, Humboldt Bay, Northwestern California. In: Conference Paper. Humboldt State University, p. 11. https://doi.org/10.13140/RG.2.1.3278.0647.

Kachel, N.B., Smith, J.D., 1986. Geologic impact of sediment transporting events on the Washington continental shelf. In: Knight, R.J., McLean, J.R. (Eds.), Shelf Sands and Sandstones. Canadian Society of Petroleum Geologists, Memoir II, pp. 145–162.

Karlin, R., 1980. Sediment sources and clay mineral distributions off the Oregon coast. J. Sediment. Res. 50, 543–559.

Kingen, K., 2021. Climatic Controls on the Kinematics of the Hooskanaden Landslide, Curery County, Oregon. M.S. Thesis. Portland State University, Portland, Oregon.

Kopp, R.E., Gilmore, E.A., Little, C.M., Lorenzo-Trueba, J., Ramenzoni, V.C., Sweet, W. V., 2019. AGU centennial grand challenge: sea-level science on the frontier of usability. earth's future. AGU Adv. Earth Space Sci. 7, 1235–1269.

Kulm, L.D., Byrne, J.V., 1966. Sedimentary response to hydrography in an Oregon estuary. Mar. Geol. 4, 85–118.

Kulm, L.D., Peterson, C.D., 1990. Preliminary evaluation of heavy mineral content of continental shelf placer deposits off Cape Blanco, Rogue River and Umpqua River. In: Open-File Report 0-89-12. State of Oregon, Department of Geology and Mineral Industries, Portland, Oregon, p. 26.
Mann, M.E., Gleick, P.H., 2015. Climate change and California drought in the 21st century. Proc. Natl. Acad. Sci. 112, 3858–3859.
Mardock, C., 1991. Mineralogy and geochemistry. In: Preliminary Resource and Environmental Data: Oregon placer minerals, Joint State-Federal Oregon Placer Minerals Technical Task Force, Oregon Department of Geology and Mineral Industries, Open-File Report 0-91-02, pp. 9–74.
Masselink, G., Russell, P., 2013. Impacts of climate change on coastal erosion. Marine climate change impacts partnership. Sci. Rev. 2013, 71–86.
Mengel, M., Levermann, A., Frieler, K., Robinson, A., Marzeion, B., Winkelmann, R., 2016. Future Sea level rise constrained by observations and long-term commitment. Proc. Natl. Acad. Sci. U. S. A. 113, 2597–2602.
Meyers, R.A., Smith, D.G., Jol, H.M., Peterson, C.D., 1996. Evidence for eight great earthquake-subsidence events detected with ground-penetrating radar, Willapa barrier, Washington. Geology 24, 99–102.
Muhs, D.R., Kelsey, H.M., Miller, G.H., Kennedy, G.L., Whelan, J.F., McInelly, G.W., 1990. Age estimates and uplift rates for late Pleistocene marine terraces: Southern Oregon portion of the Cascadia forearc. J. Geophys. Res. 95, 6685–6698.
Ogston, A.S., Guerra, J.V., Sternberg, R.W., 2004. Interannual variability of nearbed sediment flux on the Eel River shelf, northern California. Cont. Shelf Res. 24, 117–136.
PacWave, 2019. Vibracore Logs from Research Cruise MSL1903 (pdf). College of Engineering, Oregon State University, Corvallis, Oregon, p. 27.
Percy, K.L., Bella, D.A., Sutterlin, C., Klingeman, P.C., 1974. Description and Information Sources for Oregon Estuaries. Oregon Sea Grant College Program. Corvallis, Oregon, p. 294.
Percy, D.C., Peterson, C.D., Cruikshank, K.M., 1998. Collection of ephemeral data on 1997-98 beach erosion at the Capes project within the Netarts littoral cell, Oregon. In: Final Report to Hart Crower. 10 p. and CD Rom Electronic GIS Files.
Peterson, C.D., Kingen, K.E.P., 2021. Pacific Northwest Littoral Data. Dataset. https://doi.org/10.15760/geology-data.01. Accessed March 18, 2021.
Peterson, C.D., Scheidegger, K.F., 1984. Holocene depositional evolution in a small active- margin estuary of the northwestern United States. Mar. Geol. 59, 51–83.
Peterson, C.D., Vanderburgh, S., 2018a. Tidal flat depositional response to neotectonic cyclic uplift and subsidence (1–2 m) as superimposed on latest-Holocene net sea level rise (1.0 m/ka) in a large shallow mesotidal wave-dominated estuary, Willapa Bay, Washington, USA. J. Geogr. Geol. 10, 109–139.
Peterson, C.D., Vanderburgh, S., 2018b. Interconnected accommodation space controls between sand-charged shallow tidal channels and wind-wave truncated tidal flats during latest-Holocene Sea level rise (~3.0 m) in a large mesotidal wavge-dominated estuary, Grays Harbor, Washington, USA. J. Geogr. Geol. 10, 26–56.
Peterson, C.D., Scheidegger, K.F., Niem, W., Komar, P.D., 1984. Sediment composition and hydrography in six high-gradient estuaries of the northwestern United States. J. Sediment. Petrol. 54, 086–097.
Peterson, C.D., Darienzo, M.E., Pettit, D.J., Jackson, P., Rosenfeld, C., 1991. Littoral cell development in the convergent Cascadia margin of the Pacific Northwest, USA. In: Osborne, R. (Ed.), From Shoreline to the Abyss, Contributions in Marine Geology in Honor of F.P. Shepard. SEPM Special Publication, 46, pp. 17–34.
Peterson, C.D., Darienzo, M.E., Hamilton, D., Pettit, D.J., Yeager, R.K., Jackson, P.L., Rosenfeld, C.L., Terich, T.A., 1994. Cascadia beach-shoreline data base, Pacific Northwest Region, USA. In: Oregon Department of Geology and Mineral Industries Open-File Report 0-94-2, 29 p. and 3 Electronic Database Files.
Peterson, C.D., Doyle, D.L., Barnett, E.T., 2000. Coastal flooding and beach retreat from coseismic subsidence in the central Cascadia margin, USA. Environ. Eng. Geol. 6, 255–269.
Peterson, C., Stock, E., Cloyd, C., Beckstrand, D., Clough, C., Erlandson, J., Hart, R., Murillo-Jiménez Percy, D., Price, D., Reckendorf, F., Vanderburgh, S., 2006. Dating and morphostratigraphy of coastal dune sheets from the central west coast of North America. In: Oregon Sea Grant Publications, Corvallis, Oregon, 81p. PDF on CD.
Peterson, C.D., Stock, E., Price, D.M., Hart, R., Reckendorf, F., Erlandson, J.M., Hostetler, S.W., 2007. Ages, distributions, and origins of upland coastal dune sheets in Oregon, USA. Geomorphology 91, 81–102.
Peterson, C.D., Stock, E., Hart, R., Percy, D., Hostetler, S.W., Knott, J.R., 2009. Holocene coastal dune fields used as indicators of net littoral transport: West Coast, USA. Geomorphology 116, 115–134.
Peterson, C.D., Jol, H.M., Vanderburgh, S., Phipps, J.B., Percy, D., Gelfenbaum, G., 2010. Dating of late-Holocene shoreline positions by regional correlation of coseismic retreat events in the Columbia River littoral cell. Mar. Geol. 273, 44–61.
Peterson, C.D., Cruikshank, K.M., Darienzo, M.E., 2012. Coastal tectonic strain and paleoseismicity in the South Central Cascadia Margin, Oregon, USA. In: Konstantinou, Kostas (Ed.), Natural Disaster Research, Prediction and Mitigation: Earthquakes: Triggers, Environmental Impact and Potential Hazards. NOVA Open Access Publisher, New York. Chapter 1 pp 1-37. ISBN: 978-1-62081-883-1. Published online: https://www.novapublishers.com.
Peterson, C.D., Butler, V.L., Feathers, J.K., Cruikshank, K.M., 2014a. Geologic records of net littoral drift, beach plain development, and paleotsunami runup, North Sand Point, Olympic Peninsula, Washington, USA. Pacific Northwest Sci. 88, 314–328.
Peterson, C.D., Vanderburgh, S., Roberts, M., 2014b. Late Holocene geomorphology of the Columbia River Estuary, Oregon and Washington, USA. J. Geogr. Geol. 6, 1–27.
Peterson, C.D., Kingen, K.E., Erlandson, J.M., Kaijankoski, P., Meyer, J., Ryan, C., 2019. Widespread evidence of Terminated Marine Transgressive Sand Supply and Failing Longshore Sand Transport to Eroding Coastal Eolian Sand Ramps during the Latest Holocene Time in Oregon and California (Pacific Coast, USA). J. Coast. Res. 35, 1145–1163.
Peterson, C.D., Linde, T.C., Vanderburgh, S., 2020a. Late-Holocene shoreline responses to competing shelf, bay, and beach accommodation spaces under conditions of relative sea level change, and the potential for future catastrophic beach retreat in the Columbia River Littoral Cell, Washington and Oregon, USA. Mar. Geol. 427, 106272.
Peterson, C.D., Doyle, D.L., Rosenfeld, C.L., Kingen, K.E., 2020b. Predicted responses of beaches, bays, and inner-shelf sand supplies to potential sea level rise (0.5–1.0 m) in three small littoral subcells in the high-wave-energy Northern Oregon coast, USA. J. Geogr. Geol. 12, 1–27.
Pettit, D.J., 1990. Distribution of Sand within Selected Littoral Cells of the Pacific Northwest. M.S Thesis. Portland State University, Portland, Oregon.
Priest, G.R., 1999. Coastal shoreline change study northern and central Lincoln County, Oregon. In: Crowell, M., Leatherman, S.P. (Eds.), Coastal Erosion Mapping and Management. Journal of Coastal Research, Special Issue No. 28, pp. 140–157.
Rosenfeld, C.L., Peterson, C.D., Pettit, D.J., Jackson, P.L., Kimerling, A.J., 1991. Integrated photogrametric and geophysical monitoring of shoreline instability in littoral cells in the Pacific Northwest. In: ASCE Coastal Sediments 91 Proceedings, (1991), pp. 2214–2222.
Ruggiero, P., Kaminsky, G.M., Gelfenbaum, G., Cohn, N., 2016. Morphodynamics of prograding beaches: a synthesis of seasonal-to century-scale observations of the Columbia River littoral cell. Mar. Geol. 376, 51–68.
Runge, E.J., 1966. Continental Shelf Sediments, Columbia River to Cape Blanco, Oregon. Ph.D. Thesis. Oregon State University, Corvallis, Oregon.
Satake, K., Shimazaki, K., Tsuji, Y., Ueda, K., 1996. Time and size of giant earthquake in Cascadia inferred from Japanese tsunami records of January 1700. Nature 378, 246–249.
Scheidegger, K.F., Phipps, J.B., 1976. Dispersal patterns of sands in Grays Harbor estuary, Washington. J. Sediment. Petrol. 46, 163–166.
Scheidegger, K.F., Kulm, L.D., Runge, E.J., 1971. Sediment sources and dispersal patterns of Oregon continental shelf sands. J. Sediment. Petrol. 41, 1112–1120.
Schlicker, H.G., Deacon, R.J., Olcott, G.W., Beaulieu, J.D., 1973. Environmental Geology of Lincoln County Oregon. Bull. Oregon Dept. Geol. Mineral Ind. 81.
Shaw, J., Taylor, R.B., Solomon, S., Christian, H.A., Forbes, D.L., 1998. Potential impacts of global sea-level rise on Canadian coasts. Canadian Geographer/Le Géographe Canadien 42, 365–379.
Sternberg, R.W., 1986. Transport and accumulation of river-derived sediment on the Washington continental shelf, USA. J. Geol. Soc. Lond. 143, 945–956.
Stive, M.J., 2004. How important is global warming for coastal erosion? Clim. Chang. 64, 27.
Swartz, M.L., James, M., Bronson, H.S., 1985. Net shore-drift along the Pacific Coast of Washington State. Shore and Beach 53, 21–33.
Toimil, A., Losada, I.J., Camus, P., Díaz-Simal, P., 2017. Managing coastal erosion under climate change at the regional scale. Coast. Eng. 128, 106–122.
Traykovski, P., Geyer, W.R., Irish, J.D., Lynch, J.F., 2000. The role of wave-induced density-driven fluid mud flows for cross-shelf transport on the Eel River continental shelf. Cont. Shelf Res. 20, 2113–2140.
U.S. Geological Survey, 2020. USGS Lidar Point Cloud CA (20171109) WestCoastElNinoUTM10 2016 10TDU37655304 LAS 2017: U.S. Geological Survey, Lidar. Accessed August 8, 2020.
USACE, 1991a. Rogue, Oregon, Dredged Material Disposal Site Designation Final Environmental Impact Statement. Rogue Ocean Dredged Material Disposal Site (ODMDS) Designation. U.S Army Corps of Engineers and Environmental Protection Agency, Region 10, Portland District Portland, Oregon, p. 35.
USACE, 1991b. Chetco, Oregon, Dredged Material Disposal Site Designation. Draft Environmental Impact Statement. Chetco Ocean Dredged Material Disposal Site (ODMDS) Designation. U.S Army Corps of Engineers and Environmental Protection Agency, Region 10, Portland District Portland, Oregon, p. 41.
USACE, 2005a. Final Site Management/Monitoring Plan: Mouth of the Columbia River, Deep Water and Shallow Water Sites USEPA Section 102. Army Corps of Engineers, Portland District. Portland, Oregon, p. 35. Online PDF accessed May 20, 2021. https://www.epa.gov/sites/production/files/2015-10/documents/r10-_mcr_smmp_2005.pdf.
USACE, 2005b. Final Site Management/Monitoring Plan, Mouth Of The Columbia River (MCR). Shallow Water Site (SWS) and Deep Water Site (DWS). Ocean Dredge Materials Disposal Sites (ODMDS). U.S Army Corps of Engineers and Environmental Protection Agency, Region 10, Portland District Portland, Oregon, p. 35.
USACE, 2006. Site Management/Monitoring Plan, Coos Bay, Oregon, site E. F, and site H. EPA section 102. Ocean Dredge Materials Disposal Sites (ODMDS). U.S Army Corps of Engineers and Environmental Protection Agency, Region 10, Portland District Portland, Oregon, p. 19.
USACE, 2012. Yaquina Bay, Oregon, Ocean Dredged Material Disposal Sites Evaluation Study and Environmental Assessment. U.S Army Corps of Engineers and Environmental Protection Agency, Region 10, Portland District Portland, Oregon, p. 44.
Vanderburgh, S., Gelfenbaum, G., Jol, H., Kaminsky, G., Peterson, C., Phipps, J., 2003. Coastal evolution, dynamic shoreline processes, and beach management controversies of the Columbia River littoral cell, southwest Washington, and Northwest Oregon. In: Field Trip Guide #6 for Geological Society of America 2003 Annual Meeting, Seattle, Washington, p. 77.
Vanderburgh, S., Roberts, M.C., Peterson, C.D., Phipps, J.B., Herb, A., 2010. Holocene transgressive and regressive deposits of the Columbia River littoral cell barriers and beach plains. Mar. Geol. 273, 32–43.
Venkatarathnam, K., McManus, D.A., 1973. Origin and distribution of sands and gravels on the northern continental shelf of Washington. J. Sediment. Petrol. 43, 799–811.

Vousdoukas, M., Ranasinghe, R., Mentaschi, L., Plomaritis, T.A., Athanasiou, P., Luijendijk, A., Feyen, L., 2020. Sandy coastlines under threat of erosion. Nat. Clim. Change Lett. 10, 260–263.
Walkden, M., Dickson, M., 2008. Equilibrium erosion of soft rock shores with a shallow or absent beach under increased sea level rise. Mar. Geol. 251, 75–84.
Wilcoxen, P.J., 1986. Coastal erosion and sea level rise: Implications for ocean beach and San Francisco's Westside Transport Project. Coast. Manag. 14, 173–191.
Woxell, L.K., 1998. Prehistoric Beach Accretion Rates and Long-Term Response to Sediment Depletion in the Columbia River Littoral Cell. M.S. Thesis. Portland State University, Portland, Oregon.
Zhang, K., Douglas, B.C., Leatherman, S.P., 2004. Global warming and coastal erosion. Clim. Chang. 64, 41.